

Hedging Exotic Options in Stochastic Volatility and Jump Diffusion Models

ABSCHLUSSARBEIT

zur Erlangung des akademischen Grades

Master of Science

(M.Sc.)

im Masterstudiengang Statistik

an der Wirtschaftswissenschaftlichen Fakultät

Humboldt-Universität zu Berlin

von

Kai Detlefsen

geboren am 09.01.1976 in Kiel

Gutachter:

Prof. Dr. Wolfgang Härdle
PD Dr. Marlene Müller

eingereicht am Januar 27, 2005

Hedging Exotic Options in Stochastic Volatility and Jump Diffusion Models

Master Thesis submitted

to

Prof. Dr. Wolfgang Härdle

CASE - Center for Applied Statistics and Economics

Institute for Statistics and Econometrics

Humboldt-Universität zu Berlin



by

Kai Detlefsen

(158102)

in partial fulfillment of the requirements

for the degree of

Master of Science

Berlin, 7th February 2005

Declaration of Authorship

I hereby confirm that I have authored this master thesis independently and without use of others than the indicated sources. All passages which are literally or in general matter taken out of publications or other sources are marked as such.

Berlin, 7th February 2005

Kai Detlefsen

Acknowledgement

I would like to thank my Prof. Dr. Wolfgang Härdle for giving me the opportunity and motivation to write this thesis. Moreover, I would like to thank PD Dr. Marlene Müller for her stimulating course on non- and semiparametric methods.

I would also like to thank Dr. Peter Schwendner, Dr. Matthias Fengler and the Investment Banking Research Group of Bankhaus Sal. Oppenheim where I completed two internships in quantitative finance doing research on hedging. Furthermore, I would like to thank Szymon Borak for his implementation of the Simulated Annealing algorithm.

Last but not least I would like to thank Valeria Binello, my family and my friends for their encouragement and understanding all the way during this work.

Abstract

Fundamental progress has been made in developing more realistic option pricing models. While the hedging performance of these models has been investigated for plain vanilla options, it is still unknown how well these generalizations improve the hedging of exotic options. Using different barrier options on the DAX, we examine a stochastic volatility, a jump diffusion and a mixed model. We consider delta hedging, vega hedging and delta hedging with minimum variance in the Heston, the Bates and the Merton model. Thus, this work deals with the question of model selection that is nowadays of great importance because of the growing number of models and exotic products.

Contents

1	Introduction	1
2	Data	3
2.1	Descriptive statistics	3
2.2	Smoothed arbitrage free prices	7
3	Models	11
3.1	Merton model	13
3.2	Heston model	15
3.3	Bates model	16
4	Calibration	21
4.1	FFT based option pricing	22
4.2	Optimization methods	26
4.3	Calibration results	29
5	Exotic options and Greeks	41
5.1	Barrier and forward start barrier options	41
5.2	Monte Carlo	44
5.2.1	Control variates	48
5.3	Greeks	51
6	Dynamic hedging	57
7	Conclusion	65

List of Figures

2.1	Time series of mean implied volatilities for long maturities. (blue: in the money, green: at the money, red: out of the money)	5
2.2	Time series of mean implied volatilities for mean maturities. (blue: in the money, green: at the money, red: out of the money)	5
2.3	Time series of mean implied volatilities for short maturities. (blue: in the money, green: at the money, red: out of the money)	6
2.4	Mean implied volatility surface. (Left axis: time to maturity, right axis: moneyness)	6
2.5	DAX.	8
2.6	Interest rates for maturity 1 year.	8
3.1	Paths of the stock price in the Merton model for the parameters $\mu^M = 0.046$, $\sigma = 0.15$, $\lambda = 0.5$, $\delta = 0.2$ and $m = -0.243$.	14
3.2	Paths of the stock price in the Heston model for the parameters $\xi = 1.0$, $\eta = 0.15$, $\rho = -0.5$, $\theta = 0.5$ and $v_0 = 0.1$	16
3.3	Paths of the volatility in the Heston model and in the Bates model with the parameters $\xi = 1.0$, $\eta = 0.15$, $\rho = -0.5$, $\theta = 0.5$ and $v_0 = 0.1$	17
3.4	Paths of the stock price in the Bates model under the equivalent martingale measure with the parameters $\lambda = 0.5$, $\delta = 0.2$, $\bar{k} = -0.1$, $\xi = 1.0$, $\eta = 0.15$, $\rho = -0.5$, $\theta = 0.5$ and $v_0 = 0.1$	19
4.1	Implied volatility surface of the Merton model for $\mu^M = 0.046$, $\sigma = 0.15$, $\lambda = 0.5$, $\delta = 0.2$ and $m = -0.243$. (Left axis: time to maturity, right axis: moneyness)	25
4.2	Implied volatility surface of the Heston model for $\xi = 1.0$, $\eta = 0.15$, $\rho = -0.5$, $\theta = 0.5$ and $v_0 = 0.1$. (Left axis: time to maturity, right axis: moneyness)	25

4.3	Implied volatility surface of the Bates model for $\lambda = 0.5$, $\delta = 0.2$, $\bar{k} = -0.1$, $\xi = 1.0$, $\eta = 0.15$, $\rho = -0.5$, $\theta = 0.5$ and $v_0 = 0.1$. (Left axis: time to maturity, right axis: moneyness) .	26
4.4	Black Scholes vega surface.	30
4.5	Goodness of fit; Bates(blue), Heston(green) and Merton(red). .	33
4.6	Goodness of fit; Bates(blue) and Heston(green).	34
4.7	Observed and Bates model's implied volatility surface.	35
4.8	Observed and Heston model's implied volatility surface.	36
4.9	Observed and Merton model's implied volatility surface.	37
4.10	Observed and Merton model's price surface.	38
4.11	Parameter in Bates model (blue) and in the Heston model (green).	39
4.12	Parameter in Bates model (blue) and in the Merton model (red). .	40
5.1	Prices of 1y dop (black), 2y dop (blue), 1y uoc (green), 2y uoc (red), fs dop (cyan) and fs uoc (magenta)	46
5.2	Option prices per DAX in the Bates model (blue), the Heston model (green) and in the Merton model (red)	47
5.3	Correlation of the 1 year down-and-out put barrier option and the control variates: Black Scholes barrier (black), underlying (blue), European put (green), butterfly spread (red) and option with final barrier payoff (cyan).	50
5.4	Correlation of the differences of the control variates and the differences of the 1 year down-and-out barrier option; Black Scholes barrier (black), underlying (blue), European put (green), butterfly spread (red) and option with final barrier payoff (cyan). .	51
5.5	variance reduction using butterfly spreads as control variates for differences (upper line) and prices (lower line)	52
5.6	Greeks for a down-and-out put that knocks out.	54
5.7	Greeks for a down-and-out put that expires normally.	55
6.1	Hedging results for 1y dop.	59
6.2	Hedging results for 2y dop.	60
6.3	Hedging results for 1y uoc.	61
6.4	Hedging results for 2y uoc.	62
6.5	Hedging results for fs dop.	63
6.6	Hedging results for fs uoc.	64

List of Tables

2.1	Number of observations.	4
2.2	Variance- correlation table.	7
4.1	Dependence of the calibrated parameters on the input surface in the Bates model using the BFGS algorithm.	28
4.2	Dependence of the calibrated parameters on the input surface in the Bates model using simulated annealing.	28
4.3	Calibration results of the first year for the Bates model using moving starting parameters.	31
4.4	Calibration results of the first year for the Bates model using simulated annealing and BFGS.	31
4.5	Description of the time series of calibrated parameters for the Bates model using simulated annealing with 50% cooling.	32
5.1	Standard errors for Bates prices (100000 simulations).	45
5.2	Correlation between option prices and DAX.	48
5.3	Correlation between option prices per notational and at the money implied volatilities with mean time to maturity.	48

Symbols and notation

(W_t)	Wiener process
(L_t)	Lévy process
(N_t)	Poisson process
(S_t)	stock price process
(X_t)	log stock price process
(V_t)	volatility process
E	expectation
Var	variance
Cov	covariance
ψ	Fourier transform
$\mathbf{1}$	indicator function
\mathbf{i}	imaginary unit
φ	density of standard normal distribution
Φ	distribution function of standard normal distribution
$\alpha_n = o(\beta_n)$	if $\lim_{n \rightarrow \infty} \frac{\alpha_n}{\beta_n} = 0$
$\alpha_n = \mathcal{O}(\beta_n)$	if $(\frac{\alpha_n}{\beta_n})$ is bounded
x^+	$\mathbf{1}_{\{x>0\}}$

Chapter 1

Introduction

One of the major breakthroughs of finance is the Black Scholes formula. It prices European put and call options by no-arbitrage arguments and thus represents the fair price of these financial products. This way of finding a fair theoretical price had a great impact on option markets and spurred considerably their development. On the other hand the Black Scholes formula has also been celebrated in academia. This became obvious when Black and Scholes won the Nobel prize for economics in 1997 for their work.

Prices of options are measured nowadays often in implied volatilities which are derived by inversion of the Black Scholes formula. Thus implied volatilities illustrate the importance of the formula. But on the other hand they lead to one shortcoming of the Black Scholes model: Instead of being constant as is assumed by the model, the implied volatilities observed on the markets have in general a strictly convex shape - often referred to as smile. Moreover, Black's and Scholes' assumption of normally distributed returns has often to be rejected. Market returns tend to have a leptocurtic distribution.

Because of these and other deficiencies of the Black Scholes model, many extensions have been considered recently. The modern quantitative finance literature discusses for example local volatility models (e.g. Derman et al. (1994)), stochastic volatility models (e.g. Heston (1993)) and exponential Lévy models (e.g. Madan et al. (1991)). While many models fit well an observed smile curve their overall performance has often not been analyzed empirically. Thus there is a gap between theory and data.

Bakshi et al. (1997) filled this gap and compared alternative option pricing models by the hedging performance. They considered European options in models with stochastic volatility, stochastic interest rates or jumps and

concluded that the stochastic volatility models yield the best hedging performance while no other model gives better fits to the observed prices.

In this work, we want to analyze a similar problem for exotic options. We restrict ourselves to models with stochastic volatility or jumps. To this end, we have chosen from the class of stochastic volatility models the Heston model and from the class of exponential Lévy models the Merton model. This allows us to consider also the combination of these approaches, the Bates model. From the huge class of exotic options we consider six kinds of barrier options which are among the most traded products. But these exotic options are traded over the counter and thus there exist no observations of their market prices. Hence it is difficult to measure the performance of these models.

We implement the models by calibrating them on each trading day to an implied volatility surface of market prices. Thus we get for each model a time series of its parameters. Then we consider on each day an exotic option and hedge it during its life time on the basis of greeks. At expiry or knock out of the option we observe the cumulative hedging error for that option. In this way, we collect all the cumulative hedging errors for options that started on different days. Finally, we compare the hedging errors for different options, models and hedging strategies.

This work has been carried out from an applied point of view. While it makes sense to consider the prices of the options, traders speak mainly about implied volatilities. Thus we calibrate directly the implied volatility surface. Moreover, we hedge the exotic options dynamically because this is what most exotics traders do. In theory, there are objections to dynamic hedging in the models that we consider. Static hedging is for example an alternative approach that has some merits. But we follow the applied view of the traders. Theory has concentrated so far on continuous barrier options because these are easier to analyze in continuous models. But in reality the barrier can - and thus is - only checked at discrete points of time. Hence we also price and hedge the discrete barrier options. These examples illustrate that we have tried to adopt an applied standpoint in this study.

This work is organized as follows: In chapter 2, we describe the data and explain a smoothing method that we have used to delete arbitrage opportunities in the data. In chapter 3, we present the three models that we consider in this work. In chapter 4, we consider the problem of calibrating the models to the data. This gives us a time series of the model parameters and we see how well the models can replicate the data. Chapter 5 explains how we calculate the prices and the greeks of the exotic options. In chapter 6, we present the hedging results for the three models, the six options and three different hedging schemes. Finally, we discuss our conclusions in chapter 7.

Chapter 2

Data

Our empirical work is based on a time series from January 2000 to June 2004 that contains derivative prices, interest rates and the prices of the underlying. These data come from the EUREX, the German futures and stock exchange in Frankfurt.

The considered derivatives are European options on the DAX, a German stock index containing the 30 biggest German companies. As the prices of European calls and puts are linked in theory by the put call parity we work with the implied volatilities which are the values of volatility in the Black Scholes model that reproduce the observed prices. Because of the put call parity we can furthermore interpret all implied volatilities as prices of put options without loss of generality. As interest rates we use the rates at which interbank term deposits are offered between European prime banks (EURIBOR).

For each trading day of the period, we observe

- an implied volatility surface of settlement prices on a discrete strike-maturity grid
- the value of the underlying index
- the interest rate curve.

2.1 Descriptive statistics

In the following, we present some descriptive statistics of the surfaces, the underlying index and the interest rates. Moreover, we record some economic

maturity	moneyness			sum
	0.5 – 0.9	0.9 – 1.1	1.1-1.5	
1.0 – 5.0	24476	18383	21353	64212
0.25 – 1.0	37670	41047	38832	117549
0.04 – 0.25	31783	47574	29677	109034
sum	93929	107004	89862	290795

Table 2.1: Number of observations.

details of the data.

As we assume that the market for European put options on the DAX is illiquid for extreme maturities or relative strikes, we have not considered the implied volatilities for small maturities t ($t < 2$ weeks) or extreme relative strikes K/S ($K/S < 0.5$ or $K/S > 1.5$). Thus, the market in the remaining area is quite liquid and one cannot observe bid ask spreads which are the differences between the prices for selling and buying.

Moreover, the implied volatility surfaces have been preprocessed in two ways: In order to eliminate tax effects we have applied to a part of the data a method developed by Hafner et al. (2001). As the option pricing models produce arbitrage free prices it is important for the calibration to delete obvious arbitrage opportunities. To this end, we used a smoothing algorithm by Fengler (2004) which is explained in section 2.2.

In order to describe the time series of surfaces we divide the relative strike - maturity plane into nine regions: We classify the maturities t as short term ($t < 0.25$ years (S)), medium term ($0.25 \leq t < 1$ year (M)) and long term ($1 \leq t < 5$ years (L)). Similarly we classify the relative strikes K/S of the puts as "in the money" ($K/S < 0.9$ (I)), "at the money" ($0.9 \leq K/S \leq 1.1$ (A)) and "out of the money" ($1.1 < K/S$ (O)).

Then we derive for each region a time series by taking on each trading day the mean of all implied volatilities that fall in the region. These time series are given in the plots 2.1, 2.2 and 2.3. The means of these time series represent a mean surface which is depicted in figure 2.4. This mean implied volatility surface is not constant and thus is contradictory to the assumption of a constant volatility in the Black Scholes model.

Finally, we report the variances and the correlation of the time series in table 2.2 where the bold numbers represent the correlation coefficients.

Besides the implied volatility surfaces we use data about the underlying

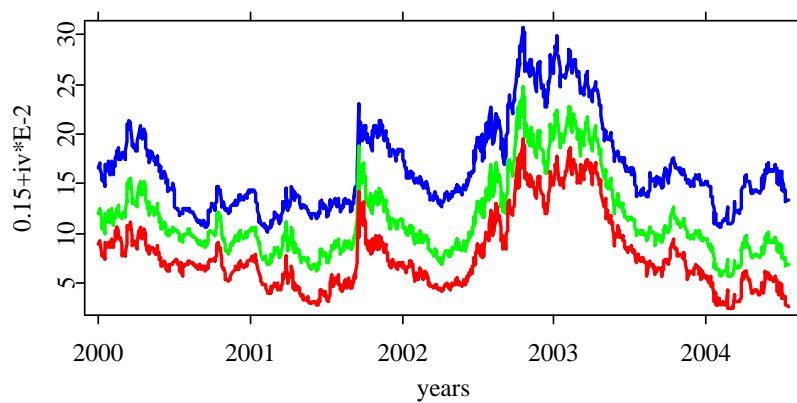


Figure 2.1: Time series of mean implied volatilities for long maturities. (blue: in the money, green: at the money, red: out of the money)

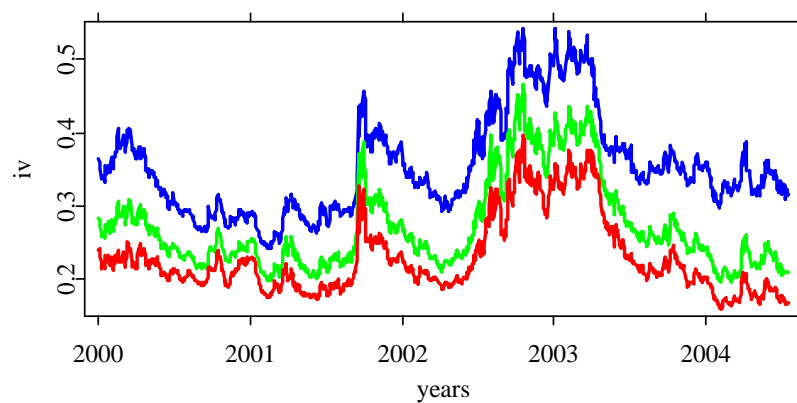


Figure 2.2: Time series of mean implied volatilities for mean maturities. (blue: in the money, green: at the money, red: out of the money)

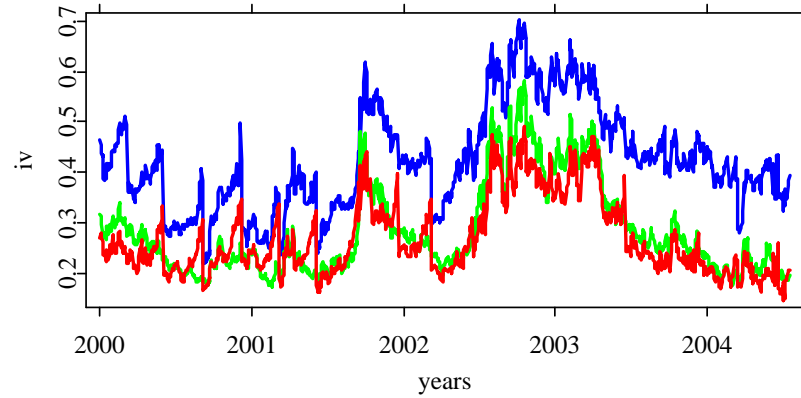


Figure 2.3: Time series of mean implied volatilities for short maturities. (blue: in the money, green: at the money, red: out of the money)

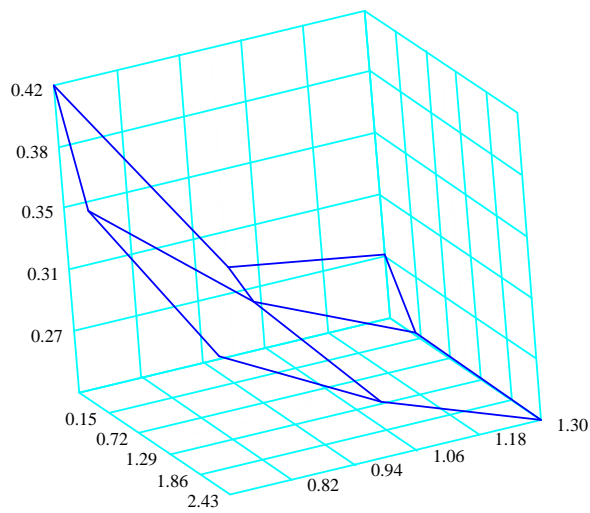


Figure 2.4: Mean implied volatility surface. (Left axis: time to maturity, right axis: moneyness)

	IL	AL	OL	IM	AM	OM	IS	AS	OS
IL	0.0020	0.0017	0.0016	0.0030	0.0027	0.0022	0.0040	0.0038	0.0027
AL	0.9626	0.0016	0.0015	0.0025	0.0024	0.0020	0.0034	0.0033	0.0025
OL	0.8690	0.9279	0.0016	0.0022	0.0022	0.0019	0.0030	0.0030	0.0023
IM	0.9618	0.9176	0.8295	0.0046	0.0040	0.0032	0.0064	0.0057	0.0041
AM	0.9615	0.9804	0.9057	0.9533	0.0037	0.0031	0.0055	0.0054	0.0041
OM	0.9400	0.9775	0.9179	0.9145	0.9895	0.0027	0.0045	0.0045	0.0035
IS	0.8687	0.8172	0.7312	0.9149	0.8808	0.8389	0.0105	0.0085	0.0066
AS	0.9241	0.9270	0.8496	0.9346	0.9747	0.9594	0.9165	0.0081	0.0061
OS	0.7949	0.8272	0.7682	0.7852	0.8673	0.8799	0.8439	0.8941	0.0058

Table 2.2: Variance-correlation table.

and interest rates. We present the prices of the DAX in figure 2.5. This plot shows clearly how the stock prices have fallen after the terror attack in New York on 2001/9/11. Moreover, it should be noted that the DAX is constructed such that the dividends of the firms in the DAX are reinvested.

In order to describe the interest rate curves we give in figure 2.6 a representative time series corresponding to maturity of 1 year. This time series is highly correlated ($\rho = 0.87$) with the DAX. As these interest rates are discrete we have transformed them to continuous compounding for option pricing.

2.2 Smoothed arbitrage free prices

The implied volatility surfaces have been smoothed in an arbitrage-free way using a methodology by Fengler (2004) that builds on the theory of natural smoothing splines.

The implied volatility surfaces that we have used consist of settlement data. Such data often contain stale data which belong to some period of the end of the trading day, and thus exhibit uncharacteristic patterns and

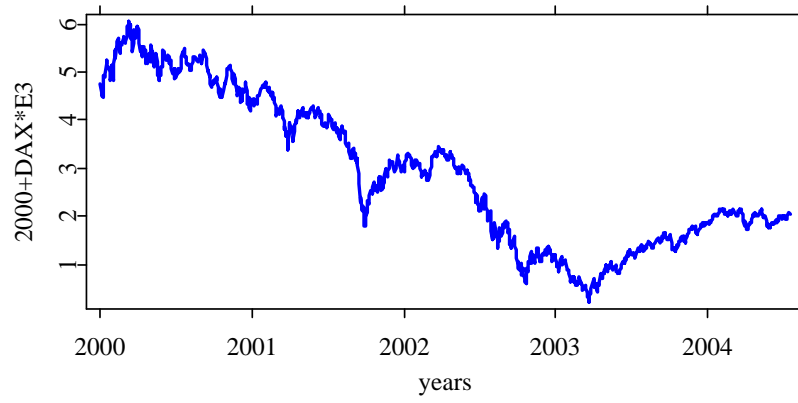


Figure 2.5: DAX.



Figure 2.6: Interest rates for maturity 1 year.

sometimes arbitrage. Therefore we have applied an arbitrage-free smoothing.

Fengler's approach minimizes the penalized sum of squares:

$$\sum_{i=1}^n w_i \{y_i - g(u_i)\}^2 + \lambda \int_a^b g''(v) dv, \quad (2.1)$$

subject to a number of linear constraints where u_i denotes a strike and y_i the corresponding call price ($i = 1, \dots, n$). The family (w_i) consists of weights and $\lambda > 0$ is a parameter determining the smoothness of the solution \hat{g} .

Denote the price of a call with strike K and maturity T by $C(S_t, t, K, T)$ where S_t is the value of the underlying at time t . Then it can be shown by differentiating that C is decreasing and convex in the strike K . Moreover, general no-arbitrage considerations proof the following bounds:

$$\max(e^{-\delta\tau} S_t - e^{-r\tau} K, 0) \leq C(S_t, t, K, T, r, \delta) \leq e^{-\delta\tau} S_t$$

where r is a continuous interest rate, δ is a continuous dividend rate and $\tau \stackrel{\text{def}}{=} T - t$ is time to maturity.

For a presentation of the spline smoothing we assume that we observe call prices y_i at strikes u_i , ($i = 0, \dots, n + 1$) where the strikes are ordered $a = u_0 < u_1 < \dots < u_{n+1} = b$. A function $g \in C^2$ is a cubic spline on $[a, b]$ if it has the representation:

$$g(u) = \sum_{i=0}^n \mathbf{1}_{[u_i, u_{i+1})}(u) s_i(u)$$

where $s_i(u) \stackrel{\text{def}}{=} d_i(u - u_i)^3 + c_i(u - u_i)^2 + b_i(u - u_i) + a_i$

for given constants a_i, b_i, c_i, d_i ($i = 0, \dots, n$). The continuity and differentiability condition impose constraints on s_i, s'_i and s''_i . Such a function g is called a natural cubic spline if $c_0 = d_0 = c_n = d_n = 0$.

There exists another representation of natural cubic splines called value second derivative representation. It is given in terms of $g_i \stackrel{\text{def}}{=} g(u_i)$ and $\gamma_i \stackrel{\text{def}}{=} g''(u_i)$ ($i = 1, \dots, n$). Let $\mathbf{g} \stackrel{\text{def}}{=} (g_1, \dots, g_n)^\top$ and $\boldsymbol{\gamma} \stackrel{\text{def}}{=} (\gamma_2, \dots, \gamma_{n-1})^\top$.

In order to formulate the minimization problem (2.1) we have to introduce some more notation: Let $h_i = u_{i+1} - u_i$ for $i = 1, \dots, n - 1$, and define the $n \times (n - 2)$ matrix \mathbf{Q} by:

$$q_{j-1,j} = h_{j-1}^{-1}, \quad q_{j,j} = -h_{j-1}^{-1} - h_j^{-1}, \quad q_{j,j+1} = h_j^{-1},$$

for $j = 2, \dots, n-1$ and $q_{i,j} = 0$ for $|i-j| > 1$. Moreover, define a symmetric $(n-2) \times (n-2)$ matrix \mathbf{R} by:

$$r_{i,i} = \frac{1}{3}(h_{i-1} + h_i), \quad r_{i,i+1} = r_{i+1,i} = \frac{1}{6}h_i,$$

for $i = 2, \dots, n-1$ and $r_{i,j} = 0$ for $|i-j| > 1$. Then the vectors \mathbf{g} and γ specify a natural cubic spline if and only if $\mathbf{Q}^\top \mathbf{g} = \mathbf{R}\gamma$. See Green et al. (1994) for details.

The minimization problem can be stated in terms of the vector $\mathbf{y} \stackrel{\text{def}}{=} (w_1 y_1, \dots, w_n y_n, 0, \dots, 0)^\top$, the vector $\mathbf{x} \stackrel{\text{def}}{=} (\mathbf{g}^\top, \gamma^\top)^\top$ and the matrices

$$\mathbf{A} \stackrel{\text{def}}{=} \begin{pmatrix} \mathbf{Q} \\ -\mathbf{R}^\top \end{pmatrix}$$

and

$$\mathbf{B} \stackrel{\text{def}}{=} \begin{pmatrix} \mathbf{W}_n & 0 \\ 0 & \lambda \mathbf{R} \end{pmatrix},$$

where $\mathbf{W}_n \stackrel{\text{def}}{=} \text{diag}(w_1, \dots, w_n)$. The solution of (2.1) is the solution of the quadratic program:

$$\begin{aligned} \min \quad & -\mathbf{y}^\top \mathbf{x} + \frac{1}{2} \mathbf{x}^\top \mathbf{B} \mathbf{x}, \\ \text{subject to} \quad & \mathbf{A}^\top \mathbf{x} = 0. \end{aligned}$$

The above described constraint, monotonicity and convexity translate into

$$\begin{aligned} \gamma_i &\geq 0, \\ \frac{y_2 - y_1}{u_2 - u_1} &\geq -e^{r\tau} \quad \text{and} \quad y_{n-1} - y_n \geq 0, \\ e^{-\delta\tau} S_t - e^{-r\tau} u_1 &\leq y_1 \leq e^{-\delta\tau} S_t \quad \text{and} \quad y_n \geq 0. \end{aligned}$$

See Fengler (2004) for details.

Finally, the function g can be computed by:

$$\begin{aligned} g(u) &= \frac{(u - u_i)g_{i+1} + (u_{i+1} - u)g_i}{h_i} \\ &\quad - \frac{1}{6}(u - u_i)(u_{i+1} - u) \left\{ \left(1 + \frac{u - u_i}{h_i}\right) \gamma_{i+1} + \left(1 + \frac{u_{i+1} - u}{h_i}\right) \gamma_i \right\}, \end{aligned}$$

for $u_i \leq u \leq u_{i+1}$, $i = 1, \dots, n-1$.

After smoothing, the whole surface can be constructed by linear construction in analogy to Kahale (2004) avoiding calendar arbitrage.

Chapter 3

Models

In the last chapter, we have described the data which also contain settlement prices of the DAX. In this chapter, we introduce some models for stock prices like the DAX. As we are interested in the problem of pricing derivatives we restrict our attention to classes that have proven to be useful in this context.

The beginning of the modern option pricing theory is often attributed to the thesis of Bachelier (1900) who modelled the stock price by a Wiener process with drift and volatility. In this framework, Bachelier was able to price options by no arbitrage arguments. But a drawback of the model is seen in the positive probability of negative stock prices.

To overcome this problem, Samuelson (1965) considered for the stock price (S_t) the exponential of Bachelier's model:

$$S_t = s_0 \exp\left\{\left(\mu - \frac{\sigma^2}{2}\right)t + \sigma W_t\right\},$$

where (W_t) is a standard Wiener process and $s_0, \mu, \sigma > 0$. The process (S_t) is called geometric Brownian motion and it is the solution of the stochastic differential equation:

$$\frac{dS_t}{S_t} = \mu dt + \sigma dW_t, \quad S_0 = s_0.$$

This equation can be interpreted economically in such a way that the stock returns dS_t/S_t consist of risk less parts μdt and normally distributed shocks σdW_t .

Samuelson's model is also known as Black-Scholes model because Black & Scholes (1973) found in this framework by no arbitrage arguments an option

pricing formula which spurred considerably the development of the option markets and was honored by the Nobel price in 1997.

The only parameter in the Black-Scholes option pricing formula that cannot be observed directly on the market is the volatility σ . Moreover, the derivative of Black Scholes option prices with respect to σ are strictly positive and thus option prices can be transformed into implied volatilities by inversion of the Black-Scholes formula. For these reasons, traders measure option prices in implied volatilities.

If Samuelson's model described correctly stock prices the implied volatilities were to be constant for different maturities and strikes. But the implied volatilities observed on the markets show - since the stock market crash in 1987 - a special pattern termed smile or skew. The smile of our data can be seen in figure 2.4. Moreover, there exist other stylized facts of financial time series that contradict assumptions of the Black-Scholes model. Real stock returns have for example often a leptokurtic and skewed distribution while the returns in Samuelson's model are normally distributed.

Because of these shortcomings several extensions have been considered: As the Wiener process is a special representant of the class of Lévy processes it is natural to consider as stock prices exponential Lévy processes:

$$S_t = \exp(L_t),$$

where (L_t) is a Lévy process. These processes allow to model jumps or to consider leptocurtic distributions. Merton (1976) followed this approach with a finite activity Lévy process while the Variance Gamma model of Madan et al. (1991) is based on an infinite activity Lévy process.

Another approach models the volatility directly by a stochastic process and hence such generalizations are called stochastic volatility models:

$$\frac{dS_t}{S_t} = \mu dt + \sqrt{V_t} dW_t,$$

where (V_t) is an (unobservable) stochastic process. Often this process (V_t) is given by another stochastic differential equation. Heston (1993) used this method and modelled the volatility by a square-root process.

A third approach considers for the stock price a diffusion process:

$$\frac{dS_t}{S_t} = \mu dt + \sigma(S_t, t) dW_t,$$

where the function σ determines the volatility at time t and price level S_t . Thus, these models are called local volatility models.

We examine in this work the Merton model, the Heston model and the Bates model which are described in more detail in the following sections. Thus we have chosen an exponential Lévy model, a stochastic volatility model and a mixture model.

3.1 Merton model

In the Black-Scholes model, the stock price process is continuous which can be interpreted economically that the prices cannot change rapidly. In order to model stock market crashes Merton (1976) extended the Black-Scholes model by adding a jump component:

$$S_t = s_0 \exp(\mu t + \sigma W_t + \sum_{i=1}^{N_t} Y_i),$$

where (N_t) is a Poisson process with intensity λ and independent jumps $Y_i \sim N(m, \delta^2)$. The Poisson process and the jumps are assumed to be independent of the Wiener process. The use of the Poisson process is economically motivated by two assumptions: the numbers of crashes in non overlapping time intervals should be independent and the occurrence of one crash should be roughly proportional to the length of the time interval.

In analogy to the Black-Scholes model the parameter μ stands in the Merton model for the expected stock return and σ is the volatility of regular shocks to the stock return. The jump component can be interpreted as a model for crashes. The parameter λ is the expected number of crashes per year and m and δ^2 determine the distribution of a single jump.

The Merton model is an exponential Lévy model because $L_t \stackrel{\text{def}}{=} \mu t + \sigma W_t + \sum_{i=1}^{N_t} Y_i$ is a Lévy process. The price process (S_t) can be interpreted as a fair game for the drift $\mu^M \stackrel{\text{def}}{=} r - \frac{\sigma^2}{2} - \lambda \{\exp(m + \frac{\delta^2}{2}) - 1\}$. This means that

$$S_t = s_0 \exp(\mu^M t + \sigma W_t^M + \sum_{i=1}^{N_t} Y_i),$$

is a martingale where $r > 0$ is the risk less interest rate.

In Section 4.1, we need the characteristic function of the logarithm of the stock price process for computing options prices by the FFT. Hence, we give

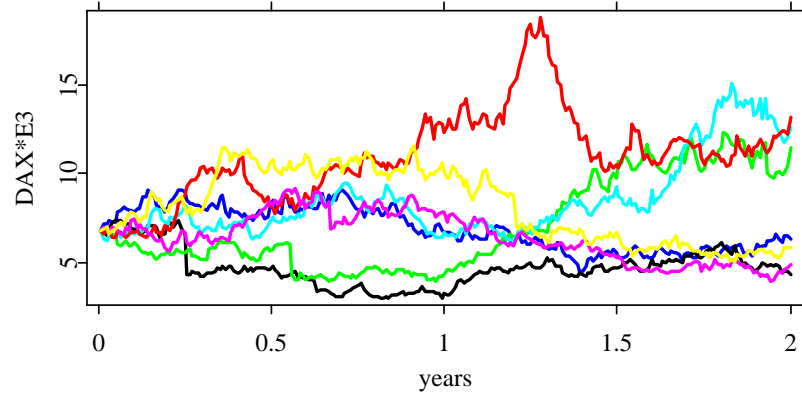


Figure 3.1: Paths of the stock price in the Merton model for the parameters $\mu^M = 0.046$, $\sigma = 0.15$, $\lambda = 0.5$, $\delta = 0.2$ and $m = -0.243$.

 [mertonsim.xpl](#)

this characteristic function:

$$\phi_{X_t}(z) = \exp\left[t\left\{-\frac{\sigma^2 z^2}{2} + \mathbf{i}\mu^M z + \lambda(e^{-\delta^2 z^2/2 + \mathbf{i}mz} - 1)\right\}\right], \quad (3.1)$$

where $X_t \stackrel{\text{def}}{=} \mu^M t + \sigma W_t^M + \sum_{i=1}^{N_t} Y_i$.

In order to compare the stock price dynamics of the Merton, Heston and Bates models we have simulated some paths based on the same model parameters. The market parameters like interest rates are taken from the first day of our data. In order to ensure comparability we have used the realizations of the random variables by using the same seed. The simulated paths of the Merton model are display in figure 3.1. Some downward jumps are clearly visible. Such jumps are the difference to the Black Scholes model which has continuous paths.

3.2 Heston model

Heston (1993) considered for the stock price a stochastic volatility model:

$$\frac{dS_t}{S_t} = \mu dt + \sqrt{V_t} dW_t^{(1)}$$

where the volatility process is modelled by a square-root process:

$$dV_t = \xi(\eta - V_t)dt + \theta\sqrt{V_t}dW_t^{(2)}$$

Here the processes $(W_t^{(1)})$ and $(W_t^{(2)})$ are correlated Wiener processes:

$$\text{Cov}\left(W_t^{(1)}, W_t^{(2)}\right) = \rho t.$$

There exists a solution to the stochastic differential equation for the volatility and it can be shown that the solution stays positive provided that $\xi\eta > \theta^2/2$. This inequality will be a nonlinear constraint in optimization in next chapter.

As usual the parameter μ stands for the expected stock return. All the other parameters determine the volatility process which cannot be observed in contrast to the stock price process. Thus, the initial condition v_0 is unknown. The parameter ξ measures the speed of mean reversion, η stands for the average level of volatility and θ is the volatility of volatility. The correlation ρ between the price shocks and the volatility shocks is in general assumed to be negative because empirical studies of financial time series confirm that volatility is negatively correlated with the returns, Cont (2001).

In this model, the dynamics of the stock price process as a martingale can be described similar to the Black-Scholes model:

$$S_t = s_0 \exp\left\{\int_0^t \left(r - \frac{1}{2}V_s\right)ds + \int_0^t \sqrt{V_s}dW_s^{(1)}\right\}.$$

For the option pricing algorithms of Section 4.1 we need the characteristic function of the logarithm of the stock price process:

$$\begin{aligned} \phi_{X_t}(z) &= \frac{\exp\left\{\frac{\xi\eta t(\xi - \mathbf{i}\rho\theta z)}{\theta^2} + \mathbf{i}ztr + \mathbf{i}zx_0\right\}}{\left(\cosh \frac{\gamma t}{2} + \frac{\xi - \mathbf{i}\rho\theta z}{\gamma} \sinh \frac{\gamma t}{2}\right)^{\frac{2\xi\eta}{\theta^2}}} \\ &\times \exp\left\{-\frac{(z^2 + \mathbf{i}z)v_0}{\gamma \coth \frac{\gamma t}{2} + \xi - \mathbf{i}\rho\theta z}\right\}, \end{aligned} \quad (3.2)$$

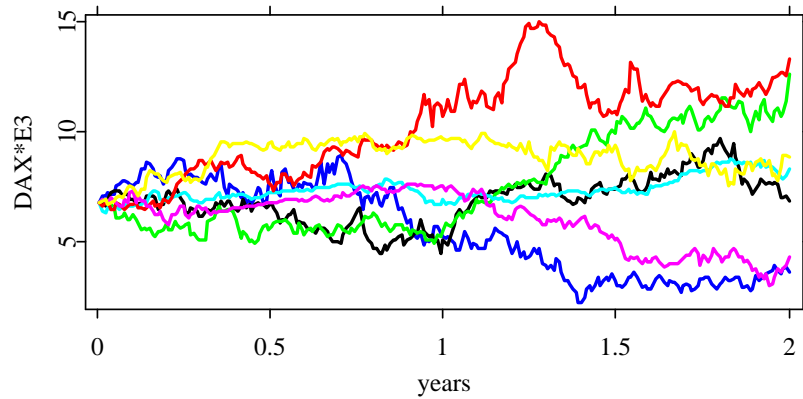


Figure 3.2: Paths of the stock price in the Heston model for the parameters $\xi = 1.0$, $\eta = 0.15$, $\rho = -0.5$, $\theta = 0.5$ and $v_0 = 0.1$.

 [hestonsim.xpl](#)

where $X_t \stackrel{\text{def}}{=} \log(S_t)$, $\gamma = \sqrt{\theta^2(z^2 + \mathbf{i}z) + (\xi - \mathbf{i}\rho\theta z)^2}$, and x_0 and v_0 are the initial values for the log-price process and the volatility process respectively.

The simulated paths of the Heston model are displayed in figure 3.2. They have no jumps but the volatility is itself a stochastic process displayed in figure 3.3.

3.3 Bates model

Merton's and Heston's approaches were combined by Bates (1996), who proposed a stock price model with stochastic volatility and jumps:

$$\begin{aligned} \frac{dS_t}{S_t} &= \mu dt + \sqrt{V_t} dW_t^{(1)} + dZ_t \\ dV_t &= \xi(\eta - V_t)dt + \theta\sqrt{V_t} dW_t^{(2)} \\ \text{Cov}\left(W_t^{(1)}, W_t^{(2)}\right) &= \rho t \end{aligned}$$

where (Z_t) is a compound Poisson process with intensity λ and independent jumps J with $\ln(1 + J) \sim N\{\ln(1 + \bar{k}) - \frac{1}{2}\delta^2, \delta^2\}$. The Poisson process is

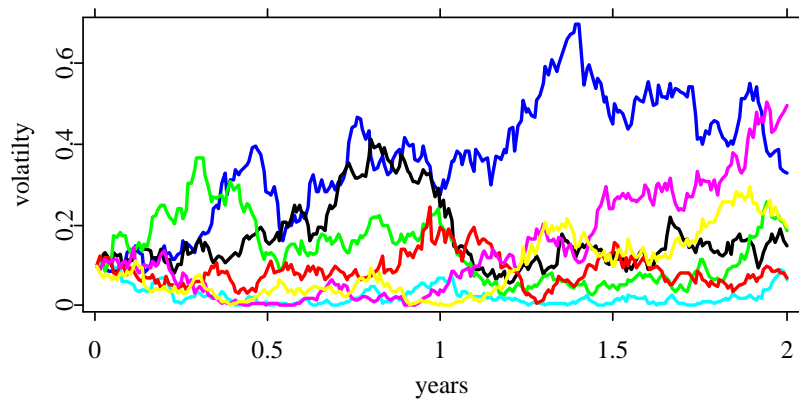


Figure 3.3: Paths of the volatility in the Heston model and in the Bates model with the parameters $\xi = 1.0$, $\eta = 0.15$, $\rho = -0.5$, $\theta = 0.5$ and $v_0 = 0.1$.

 [volasim.xpl](#)

assumed to be independent of the Wiener processes.

The parameters have in this model the same meaning as in the Heston model. Only the parameters \bar{k} and δ determine the distribution of the jumps.

Under the risk neutral probability one obtains the equation for the logarithm of the asset price:

$$dX_t = (r - \lambda\bar{k} - \frac{1}{2}V_t)dt + \sqrt{V_t}dW_t^{(1)} + \tilde{Z}_t,$$

where \tilde{Z}_t is a compound Poisson process with normal distribution of jumps.

Since the jumps are independent of the diffusion part, the characteristic function for the log-price process can be obtained as:

$$\phi_{X_t}(z) = \phi_{X_t}^D(z)\phi_{X_t}^J(z)$$

where :

$$\begin{aligned} \phi_{X_t}^D(z) &= \frac{\exp\left\{\frac{\xi\eta t(\xi - \mathbf{i}\rho\theta z)}{\theta^2} + \mathbf{i}zt(r - \lambda\bar{k}) + \mathbf{i}zx_0\right\}}{\left(\cosh \frac{\gamma t}{2} + \frac{\xi - \mathbf{i}\rho\theta z}{\gamma} \sinh \frac{\gamma t}{2}\right)^{\frac{2\xi\eta}{\theta^2}}} \\ &\times \exp\left\{-\frac{(z^2 + \mathbf{i}z)v_0}{\gamma \coth \frac{\gamma t}{2} + \xi - \mathbf{i}\rho\theta z}\right\} \end{aligned} \quad (3.3)$$

is the characteristic function of the diffusion part and

$$\phi_{X_t}^J(z) = \exp\left\{t\lambda\left(e^{-\delta^2 z^2/2 + \mathbf{i}(\ln(1+\bar{k}) - \frac{1}{2}\delta^2)z} - 1\right)\right\} \quad (3.4)$$

is the characteristic function of the jump part.

Note that (3.2) and (3.3) are quite similar. The difference lies in the shift $\lambda\bar{k}$. The formula (3.4) exposes also a similar structure as the jump part in (3.1).

The simulated paths of the Bates model are displayed in figure 3.4. They combine features of the Merton and the Heston model: They have jumps like the Merton model and a stochastic volatility as the trajectories in the Heston model. The corresponding paths of the volatility process are displayed in figure 3.3 and coincide the volatility paths for the Heston model because we have used the same seeds.

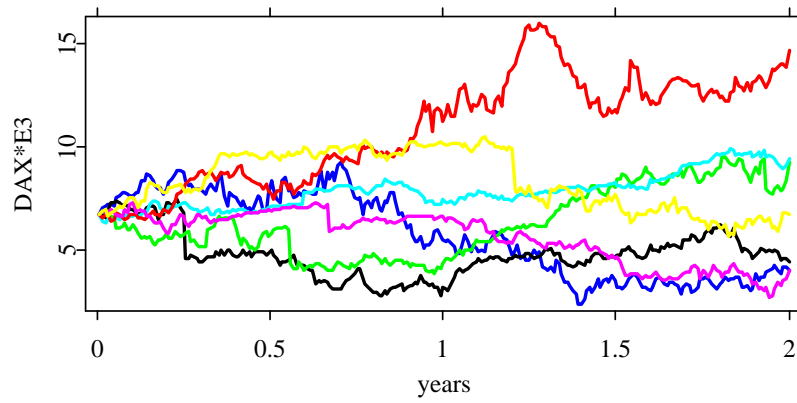


Figure 3.4: Paths of the stock price in the Bates model under the equivalent martingale measure with the parameters $\lambda = 0.5$, $\delta = 0.2$, $\bar{k} = -0.1$, $\xi = 1.0$, $\eta = 0.15$, $\rho = -0.5$, $\theta = 0.5$ and $v_0 = 0.1$.

 batessim.xpl

Chapter 4

Calibration

In the last chapter, we have introduced three stock price models. Thus, given the parameters we can model the price dynamics and value options on the stock. In this chapter, we discuss the inverse problem: Given the option prices that have been described in chapter 2 we want to find for each model parameters that replicate the observed prices. This inverse problem is known as calibration of option pricing models.

In general, an inverse problem is called ill-posed if the solution is not unique or if it does not depend continuously on the input data. Moreover, it is always important to have an efficient and stable algorithm for the implementation.

The calibration of option prices is an ill-posed problem: It is quite unlikely that any model can replicate exactly the observed prices. Thus, there is no direct solution. In order to overcome this problem we will minimize an error functional which measures some goodness of fit. To this minimization problem exist on the other hand in general many solutions. Hence, the solution of the calibration is not unique. As there are many possible solutions the solution cannot in general depend continuously on the observed prices. But in Section 4.2, we show to what extent our results are stable.

As the data is a time series the calibration yields a time series of model parameters and we face the problem of continuity of these parameters. This issue is similar to the continuous dependence discussed above. The difference lies in the fact that as time evolves not only the implied volatility changes but also other market parameters vary and maybe events occur that influence the models and their parameters.

An estimation of the model parameters based on historical stock prices leads to the physical probability measure that governs the price process.

But as we are interested in pricing and hedging of options we need instead an equivalent martingale measure that is consistent with the observed prices. Thus, it is essential to have a fast algorithm for the computation of the prices of European options. In the next section, we describe such an algorithm. Then we consider procedures for the minimization of the error functional. In the last section we combine the algorithms for calibrations and discuss the results.

4.1 FFT based option pricing

In this section, we describe a variant of an option pricing algorithm that has been introduced by Carr & Madan (1999). This numerical approach for European calls is based on the FFT and the characteristic functions of price processes. The use of the FFT is motivated by several reasons: On the one hand, the algorithm offers a speed advantage. This effect is even boosted by the possibility of the pricing algorithm to calculate prices for a whole range of strikes. On the other hand, the characteristic function of the log price process is often known analytically and has a simple form while the density is frequently unknown or complicated.

Thus, the approach assumes that the characteristic function of the log price process is given analytically. The basic idea of the method is to develop an analytic expression for the Fourier transform of the option price and then to get the price back by Fourier inversion. As the Fourier transform and its inversion work for square-integrable functions according to Plancherel's theorem we do not consider directly the option price but a modification of it.

Let $C_T(k)$ denote the price of a European call option with maturity T and strike $K = \exp(k)$. Let (S_t) denote the price process of the underlying. Then the value of the option is given by:

$$C_T(k) = \int_k^\infty e^{-rT} (e^s - e^k) q_T(s) ds$$

where q_T is a risk-neutral density of $s_T = \log S_T$.

The function C_T is not square-integrable because $C_T(k)$ converges to S_0 for $k \rightarrow -\infty$. Hence, we consider the modified function:

$$c_T(k) = \exp(\alpha k) C_T(k)$$

which is square-integrable for a suitable $\alpha > 0$. The choice of α may depend on the model for (S_t) . The Fourier transform of c_T is defined by:

$$\psi_T(v) = \int_{-\infty}^{\infty} e^{ivk} c_T(k) dk.$$

The expression for ψ_T can be computed directly after an interchange of integrals:

$$\begin{aligned} \psi_T(v) &= \int_{-\infty}^{\infty} e^{ivk} \int_k^{\infty} e^{\alpha k} e^{-rT} (e^s - e^k) q_T(s) ds dk \\ &= \int_{-\infty}^{\infty} e^{-rT} q_T(s) \int_{-\infty}^s (e^{\alpha k+s} - e^{(\alpha+1)k}) e^{ivk} dk ds \\ &= \int_{-\infty}^{\infty} e^{-rT} q_T(s) \left\{ \frac{e^{(\alpha+1+iv)s}}{\alpha + \mathbf{i}v} - \frac{e^{(\alpha+1+iv)s}}{\alpha + 1 + \mathbf{i}v} \right\} ds \\ &= \frac{e^{-rT} \phi_T\{v - (\alpha + 1)\mathbf{i}\}}{\alpha^2 + \alpha - v^2 + \mathbf{i}(2\alpha + 1)v} \end{aligned}$$

where ϕ_T is the Fourier transform of q_T . A sufficient condition for c_T to be square-integrable is given by $\psi_T(0)$ being finite. This is equivalent to

$$E(S_T^{\alpha+1}) < \infty.$$

A value $\alpha = 0.75$ fulfills this condition for the models of chapter 3. With this choice, we follow Schoutens et al. (2004) who found out in an empirical study that this value leads to stable algorithms, i.e. the prices are well replicated for many model parameters.

Now, we get the desired option price in terms of ψ_T by the Fourier inversion

$$C_T(k) = \frac{\exp(-\alpha k)}{\pi} \int_0^{\infty} e^{-ivk} \psi(v) dv.$$

This integral can be computed numerically by:

$$C_T(k) \approx \frac{\exp(-\alpha k)}{\pi} \sum_{j=0}^{N-1} e^{-iv_j k} \psi(v_j) \eta \quad (4.1)$$

where $v_j \stackrel{\text{def}}{=} \eta j$, $j = 0, \dots, N-1$ and $\eta > 0$ is the distance of the points of the integration grid.

Formula (4.1) suggests to calculate the prices by the FFT which is an efficient algorithm for computing the sums

$$w_u = \sum_{j=0}^{N-1} e^{-\mathbf{i} \frac{2\pi}{N} j u} x_j, \text{ for } u = 0, \dots, N-1$$

In general, strikes near the spot price are of interest because such options are traded for the most part. We consider thus an equidistant spacing of the log strikes around the log spot price s_0 :

$$k_u = -\frac{1}{2}N\zeta + \zeta u + s_0, \text{ for } u = 0, \dots, N-1$$

where $\zeta > 0$ denotes the distance between the log strikes. Substituting these log strikes in the approximation yields for $u = 0, \dots, N-1$

$$C_T(k_u) \approx \frac{\exp(-\alpha k)}{\pi} \sum_{j=0}^{N-1} e^{-i\zeta\eta ju} e^{i\{(\frac{1}{2}N\zeta - s_0)v_j\}} \psi(v_j)\eta.$$

Now, the FFT can be applied to

$$x_j = e^{i\{(\frac{1}{2}N\zeta - s_0)v_j\}} \psi(v_j), \text{ for } j = 0, \dots, N-1$$

provided that

$$\zeta\eta = \frac{2\pi}{N}.$$

This constraint however leads to the following trade-off: The parameter N controls the computation time and thus is often determined by the problem. So the right hand side may be regarded as given or fixed. One would like to choose a small ζ in order to get many prices for strikes near the spot price. But the constraint implies then a big η giving a coarse grid for integration. So we face a trade-off between accuracy and the number of interesting strikes.

The described algorithm offers a considerable speed advantage in comparison to Monte Carlo simulations (see e.g. (Borak et al. 2004)). The obtained implied volatilities for the Merton, Heston and Bates model are given in the following figures 4.1, 4.2 and 4.3. We have used $N = 2^{10} = 1024$ grid points for the numerical integration with a distance $\eta = 0.12$. Moreover, we have used $\alpha = 0.75$ as integrability factor as proposed by Schoutens et al. (2004). In order to obtain an equidistant grid we have interpolated the prices linearly. This procedure may result in non convex ragged curves. But as the figures show the implied volatility surfaces retain their characteristic form if the FFT parameters are chosen carefully.

The implied volatility surface of the Merton model 4.1 shows a peak at the money for short maturities. If the prices are computed more precisely this peak becomes smoother but the characteristic form remains. In general, market smiles do not form such extreme peaks. Moreover, the implied

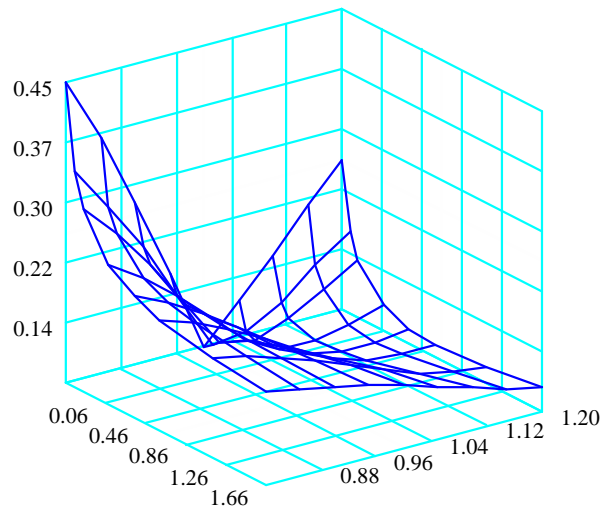


Figure 4.1: Implied volatility surface of the Merton model for $\mu^M = 0.046$, $\sigma = 0.15$, $\lambda = 0.5$, $\delta = 0.2$ and $m = -0.243$. (Left axis: time to maturity, right axis: moneyness)

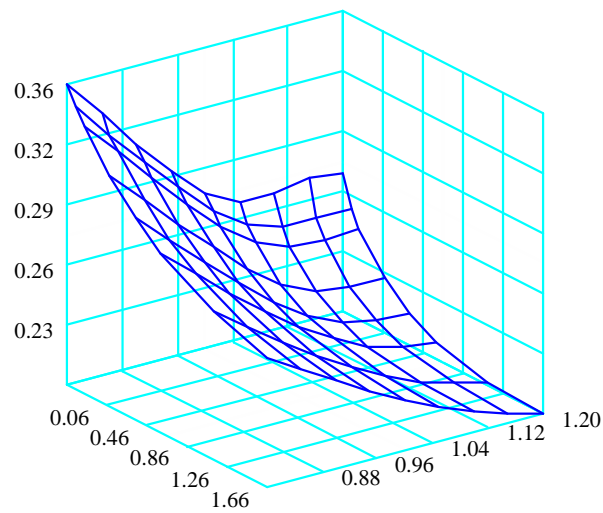


Figure 4.2: Implied volatility surface of the Heston model for $\xi = 1.0$, $\eta = 0.15$, $\rho = -0.5$, $\theta = 0.5$ and $v_0 = 0.1$. (Left axis: time to maturity, right axis: moneyness)

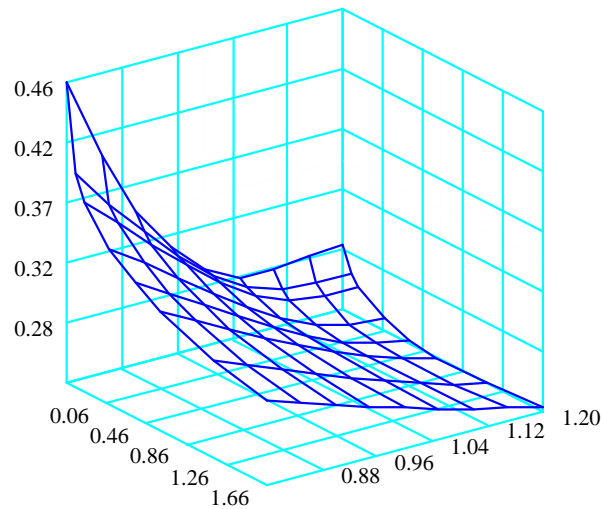


Figure 4.3: Implied volatility surface of the Bates model for $\lambda = 0.5$, $\delta = 0.2$, $\bar{k} = -0.1$, $\xi = 1.0$, $\eta = 0.15$, $\rho = -0.5$, $\theta = 0.5$ and $v_0 = 0.1$. (Left axis: time to maturity, right axis: moneyness)

volatilities increase at the money for longer time to maturity. This pattern is also observed only seldom on the markets. Thus, these two features can be interpreted as deficiencies of the Merton model.

The implied volatility surface of the Heston model 4.2 is more similar to surfaces observed on the market because the implied volatilities decrease for increasing time to maturity. Furthermore, in this surface the smile flattens with increasing time to maturity. This feature can be regarded as a stylized fact of implied volatility surfaces.

The implied volatility surface of the Bates model 4.3 is similar to the surface of the Heston model 4.2. Thus for these model parameters the stochastic volatility is more relevant for pricing than the jump part. Moreover, the prices in the Bates model are - for these parameters - higher than in the Heston model because of the additional jump risk.

4.2 Optimization methods

In order to find parameters that minimize an error functional we have to use numerical minimization algorithms. A variety of such routines has been

produced for different problems. These methods can be divided into the two classes of local and global minimization algorithms. We consider from both classes one algorithm and try to assess which of the two classes works better for the calibration of option prices. As a global routine we have chosen the simulated annealing algorithm and as local method we use the Broyden-Fletcher-Goldfarb-Shanno algorithm.

In order to measure the performance of these algorithms on simulated data we have considered the implied volatility surface of the Bates model 4.3 that has been generated from known parameters. Then we have taken this surfaces as given input and tried to reproduce the parameters.

To this end, we have applied the two minimization routines with starting parameters that have been chosen randomly in the neighborhood of the known parameters. As error functional we have used the sum of the squared errors on a moneyness-maturity grid.

We have considered the mean performance of the minimization algorithms for the Bates model for ten vectors of starting parameters. The gradient based method performs well for starting parameters near the solution. But the bigger this distance becomes the worse is the result and the longer takes the minimization. In contrast the simulated annealing algorithm always needs the same computation time because it can be controlled explicitly by parameters of the algorithm. Moreover, it performs worse in simple situations and better for difficult starting parameters compared to the BFGS algorithm.

Finally, we want to analyze by an example the dependence of the calibrated parameters on the input surface. To this end, we apply the two minimization routines to surfaces that lie $a = 1\%$, 2% , 3% , 4% or 5% over the given simulated surface. These changes retain the structure of the implied volatility surface so that no arbitrage appears.

The parameters of the given Bates surface are $\lambda = 0.5$, $\delta = 0.2$, $\bar{k} = -0.1$, $\xi = 1.0$, $\eta = 0.15$, $\rho = -0.5$, $\theta = 0.5$ and $v_0 = 0.1$. The calibrated parameters using the BFGS algorithm are given in table 4.1. Some parameters like the expected number of jumps per year λ stay quite constant while others like the standard deviation of the distribution of the jumps δ change by almost 50% for the highest implied volatility surface. But the parameters show in general a continuous dependence. Moreover, the fit which is defined in section 4.3 is always quite good although the error increases with the shift of the surface.

The results for simulated annealing are given in table 4.2. The parameters change more than in the BFGS case. More important, they do not change continuously but somehow randomly. This feature comes from the stochastic

a	λ	δ	\bar{k}	ξ	η	ρ	θ	v_0	fit
0.01	0.50	0.22	-0.10	0.99	0.15	-0.49	0.52	0.11	0.00004
0.02	0.50	0.22	-0.11	0.97	0.16	-0.47	0.54	0.11	0.00010
0.03	0.49	0.24	-0.12	0.96	0.17	-0.46	0.57	0.12	0.00021
0.04	0.48	0.24	-0.13	0.96	0.17	-0.44	0.58	0.12	0.00047
0.05	0.48	0.28	-0.13	1.04	0.17	-0.44	0.59	0.13	0.00048

Table 4.1: Dependence of the calibrated parameters on the input surface in the Bates model using the BFGS algorithm.

a	λ	δ	\bar{k}	ξ	η	ρ	θ	v_0	fit
0.01	0.94	0.10	-0.10	1.33	0.14	-0.38	0.56	0.11	0.087
0.02	0.12	0.06	-0.26	0.83	0.17	-0.45	0.35	0.11	0.030
0.03	0.46	0.17	-0.13	0.86	0.19	-0.54	0.43	0.12	0.034
0.04	0.32	0.34	-0.14	1.53	0.18	-0.67	0.39	0.12	0.009
0.05	0.90	0.19	-0.11	0.78	0.18	-0.54	0.49	0.11	0.060

Table 4.2: Dependence of the calibrated parameters on the input surface in the Bates model using simulated annealing.

nature of the simulated annealing algorithm. In addition, the goodness of fit does not show any structure and is always worse than the fits using the BFGS method. So in this theoretical comparison the BFGS algorithm seems to be more suitable for our problem.

4.3 Calibration results

In the last two sections, we have introduced the tools necessary for the calibration of implied volatility surfaces. In this section we apply these methods and choose an approach that performs well with respect to goodness of fit, speed and stability of parameters.

Before we can examine the performance of the optimization algorithms we have to decide on the error functional to be minimized: Although the prices are the real variables we use the implied volatilities for calibration because traders are mainly interested in these variables. As an analysis of our data has shown that there are no outliers in the implied volatility surfaces we measure the error basically by the squared distance between the observed implied volatilities σ^{obs} and the implied volatilities of the model σ^{mod} . The number of observed points per day is not constant because the number of maturities and the number of strikes per maturity vary. Thus, we use weights to make the errors comparable for the time series. To this end, we give every maturity of a surface the same weight such that the weights add to 1. In order to make the maturities comparable the points for each maturity get equal weights such that their sum gives the weight of the maturity. Finally we multiply every weight by the Black Scholes vega to reflect the bigger importance of at the money observations with long time to maturity for our study. The vega of an option with K strike and τ time to maturity is given by:

$$V(K, \tau) \stackrel{\text{def}}{=} S\sqrt{\tau}\varphi\left(\frac{\log(S/K) + (r - \frac{1}{2}\sigma^2)\tau}{\sigma\sqrt{\tau}}\right)$$

where φ is the density of the standard normal distribution, S spot price and σ (implied) volatility. A vega surface is given in figure 4.4 for illustration.

Thus, the error functional fit is given by:

$$fit(p) \stackrel{\text{def}}{=} \sum_{\tau} \sum_K \frac{1}{n_{\tau}n_S(\tau)} V(K, \tau) \{\sigma^{mod}(K, \tau, p) - \sigma^{obs}(K, \tau)\}^2$$

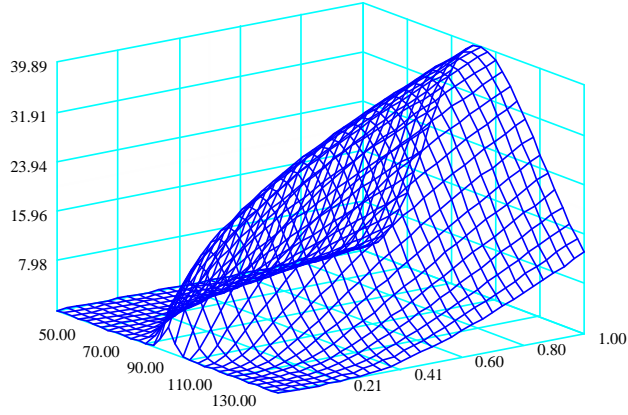


Figure 4.4: Black Scholes vega surface.

where p is a vector of model parameters, n_τ is the number of times to maturity of the observed surface and $n_S(\tau)$ is the number of strikes with time to maturity τ . The first sum is taken over all times of maturity τ of the observed implied volatility surface and the second is taken over all strikes K for that there are observations with strike K and time to maturity τ .

The model parameters that are collected in the vector p have to satisfy the natural constraints of their domains, e.g. the expected number of jumps per year λ should be positive. Moreover, we use the constraint $\xi\eta > \frac{\theta^2}{2}$ which ensures that the volatility process stays positive.

In our comparison of minimization methods we restrict our attention to the Bates model because the Merton and the Heston model can be regarded as special cases of the Bates model. Moreover, we had to restrict ourselves to the first year of the data in order to keep the computation reasonable. But we assume that the result of this period holds for the whole data.

For both algorithms we use the same starting parameters which have been chosen in the neighborhood of a local minimum of first implied volatility surface. As starting parameters for the next surface we use the calibrated parameters of the last day in order to get a continuous time series of parameters. While the BFGS algorithm has no tuning parameters the performance and the computation time of simulated annealing depend on the starting temperature, the number of iteration for each temperature and the cooling scheme. We test three cooling schemes where the temperature is reduced by 30%, 50% or 70%. First we judge the algorithms which have both been coded

algorithm	mean of fit	median of fit	computation time [min]
BFGS	1.28	0.79	247
SA30	1.33	0.77	214
SA50	1.24	0.76	222
SA70	1.32	0.76	209

Table 4.3: Calibration results of the first year for the Bates model using moving starting parameters.

algorithm	mean of fit	median of fit	computation time [min]
SA30BFGS	1.31	0.77	297
SA50BFGS	1.32	0.76	284
SA70BFGS	1.32	0.76	268

Table 4.4: Calibration results of the first year for the Bates model using simulated annealing and BFGS.

in C++ only by the goodness of fit and the speed. Table 4.3 shows that the simulated annealing algorithm is in general faster than the BFGS method (for our simulated annealing parameters). Moreover, it provides a better fit to the data. In the simulated annealing class the cooling scheme with 50% temperature reduction gives the best fit in the mean while the medians are all similar. The computation times for the three cooling schemes differ only slightly. The table leaves the question open if the local minimization routine is trapped in a local minimum or if the simulated annealing finds a global minimum valley without going exactly to the minimum in this valley. The minimizations which are described in table 4.4 applied for each implied volatility surface first a simulated annealing algorithm and then the BFGS method. The starting parameters were again the calibrated parameters of the last day. The table demonstrates that the global optimization algorithm finds a minimum and can not be improved by a local minimization after the global. This implies furthermore that the BFGS method of table 4.3 was not trapped in a local minimum. On the basis of these results we have chosen

parameter	mean μ	variance σ^2	$\frac{\sigma}{\ \mu\ }$
λ	0.40	0.33	1.45
δ	0.26	0.01	0.37
\bar{k}	0.01	0.76	0.62
ξ	0.87	3.56	2.16
η	0.15	0.03	1.22
ρ	-0.65	0.02	0.23
θ	0.33	0.04	0.61
v_0	0.05	0.00	0.41

Table 4.5: Description of the time series of calibrated parameters for the Bates model using simulated annealing with 50% cooling.

the simulated annealing algorithm with 50% cooling for our calibration.

But we are also interested in the sequence of parameters and especially their stability. Table 4.5 shows the mean, the variance and the standardized deviation of the calibrated parameters in the Bates model. The mean reversion speed ξ of the volatility process varies the most according to the standardized deviation. As this variable has no direct economic interpretation that could justify such behavior we have tried to find more stable parameter sequences by calibrating them always from the same starting parameters. Another approach was to set the variable ξ to a constant. Thus we have removed this variable from the model meaning that it is not parameterized parsimoniously. Finally, we have tested a method that regularizes the error functional by a penalty term that measures the distance to the parameters of the last calibration. We have used this penalty function and not the usual relative entropy because traders prefer to keep the change in the parameters small.

The regularization method did not improve the calibration because either the fit was relatively bad or the result was similar to the not regularized optimization. The calibration with constant starting parameters gave a fit similar to the fit above but the stability of the parameters did not improve. The Bates model with constant mean reversion led to a better mean fit but a worse median fit. The stability of the parameters became better for all

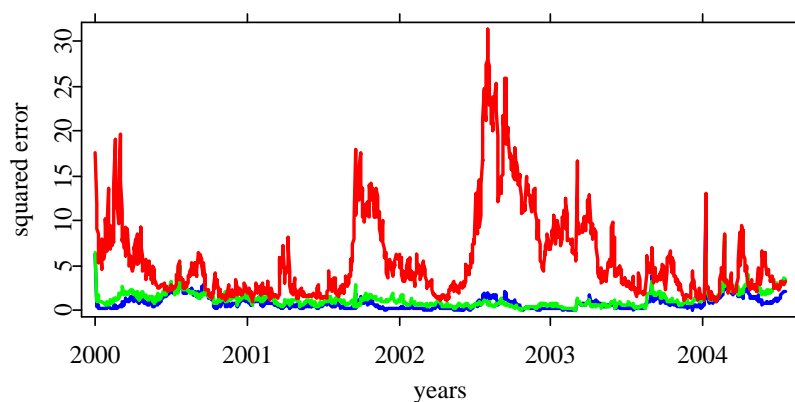


Figure 4.5: Goodness of fit; Bates(blue), Heston(green) and Merton(red).

parameters but the expected number of jumps per year. Reducing the model even more by setting the number of expected jumps or the correlation to a constant leads to bad fits. Thus, we use for the calibration the simulated annealing algorithm with 50% cooling with a constant mean reversion and as starting parameters the calibrated parameters of the last day.

Figures 4.5 and 4.6 show the goodness of fit for the whole data. The result of the Merton model is considerably worse than the other fits. This may indicate that the Merton model has problems in replicating implied volatility surfaces with long times to maturity. The fit of Heston model is a bit worse than the one of the Bates model but both seem to be influenced slightly by numerical problems. As the Bates model is a generalization of the other two models its fit should be the best. But it is interesting that the Bates model seems quite similar to the Heston. This may indicate that the stochastic volatility part is more relevant for a good fit.

The figures 4.7, 4.8 and 4.9 show the fit to the observed implied volatility surface on 25/05/2000. On this day the fits of the model are roughly at the median level of the time series. The use of the vega weights is clearly visible because the fit for long times to maturity is better than for short maturities. In order to demonstrate the importance of calibrating implied volatilities instead of prices we show in figure 4.10 the corresponding fit of the prices for the Merton which has the worst fit on 25/05/2000.

Finally, we present in this chapter the calibrated parameters for the three models. In figure 4.11 we compare the Heston model with the stochastic volatility part of the Bates model. The mean reversion speed of the Heston model oscillates around the fixed level of the Bates model. The average

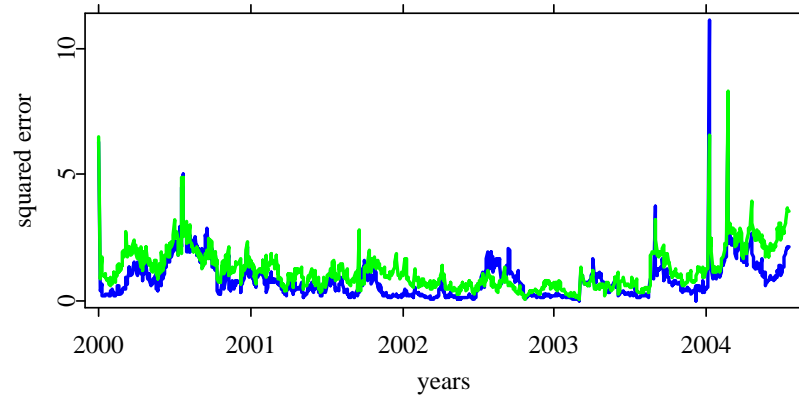


Figure 4.6: Goodness of fit; Bates(blue) and Heston(green).

volatilities are strongly correlated although this parameter is always higher in the Heston model. The correlation between spot and volatility process shows that the parameters in the Bates model are not stable. The volatility of volatility is similar in the model but the instant volatility is almost identical. In figure 4.12 the jump diffusion part of the Bates model is compared to the Merton model. All parameters are quite similar but influenced by numerical problems which lead to instability of the parameters.

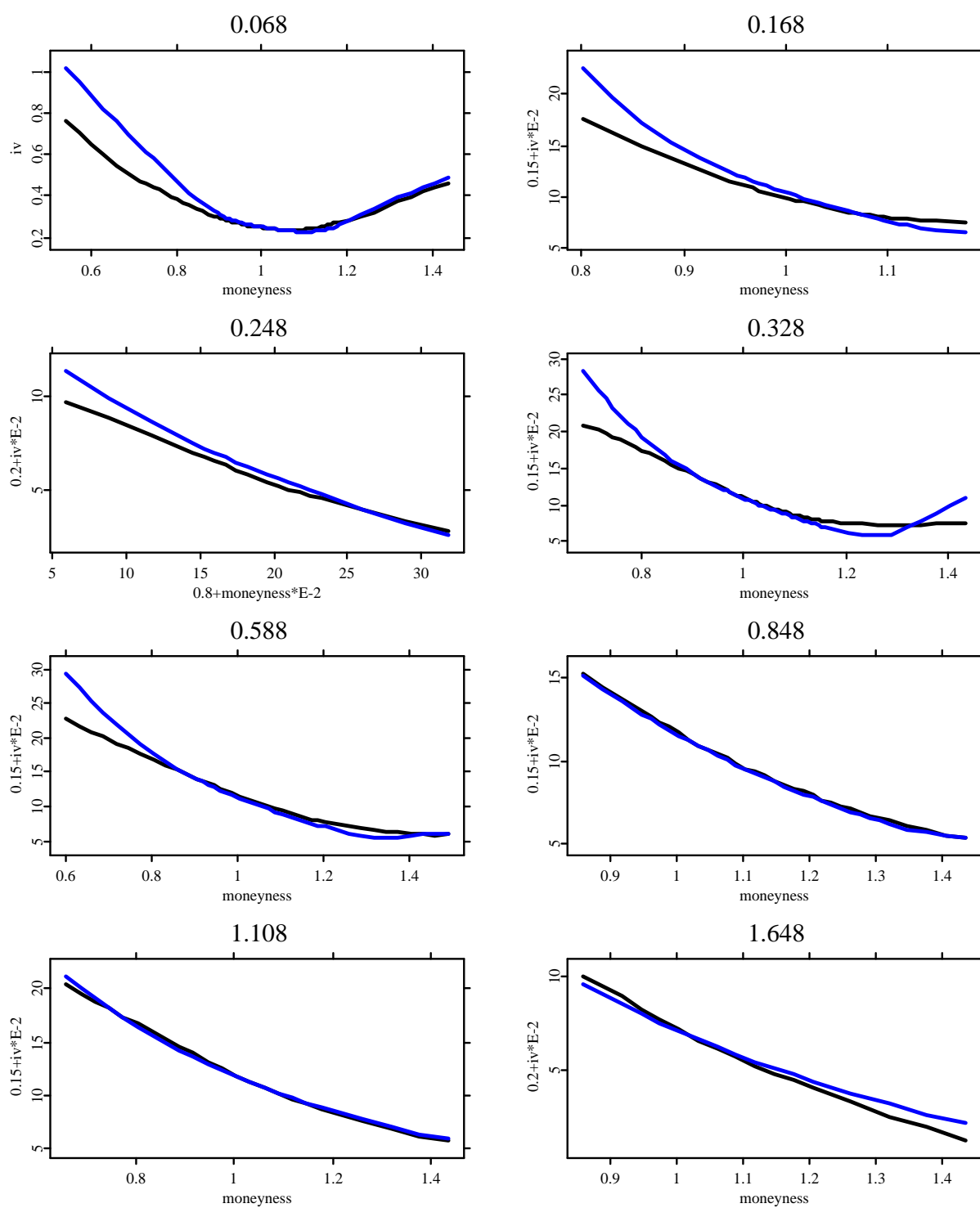


Figure 4.7: Observed and Bates model's implied volatility surface.

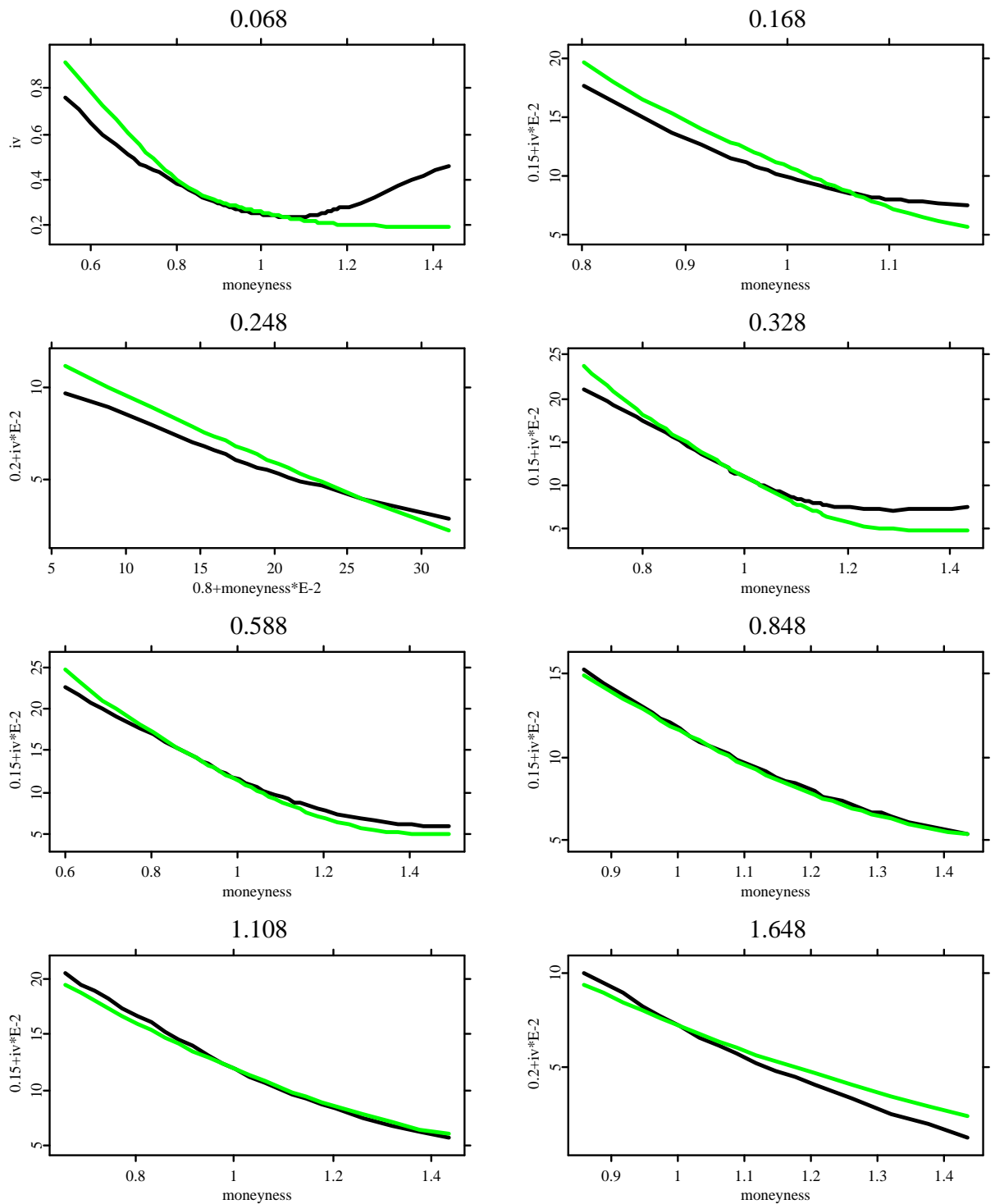


Figure 4.8: Observed and Heston model's implied volatility surface.

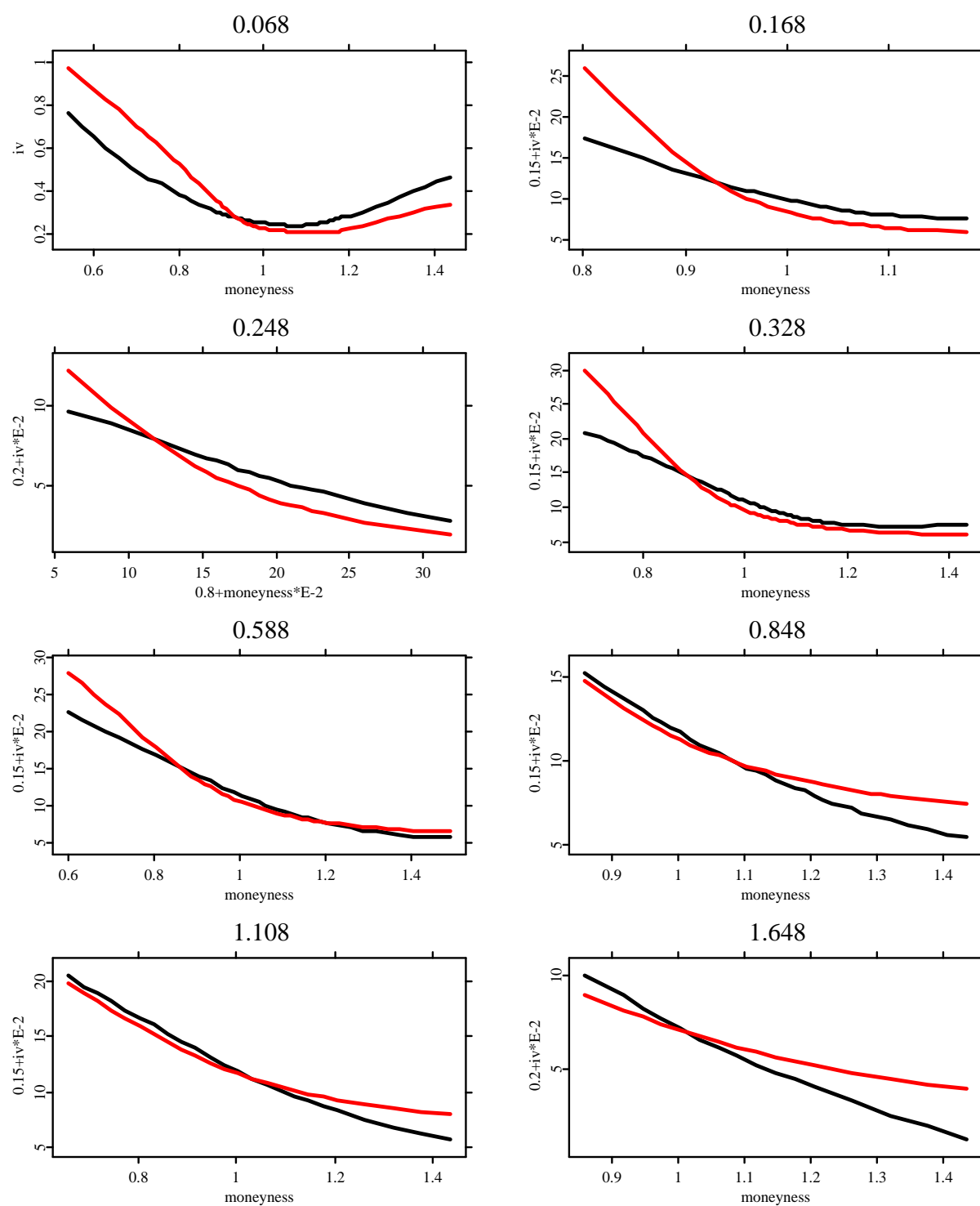


Figure 4.9: Observed and Merton model's implied volatility surface.

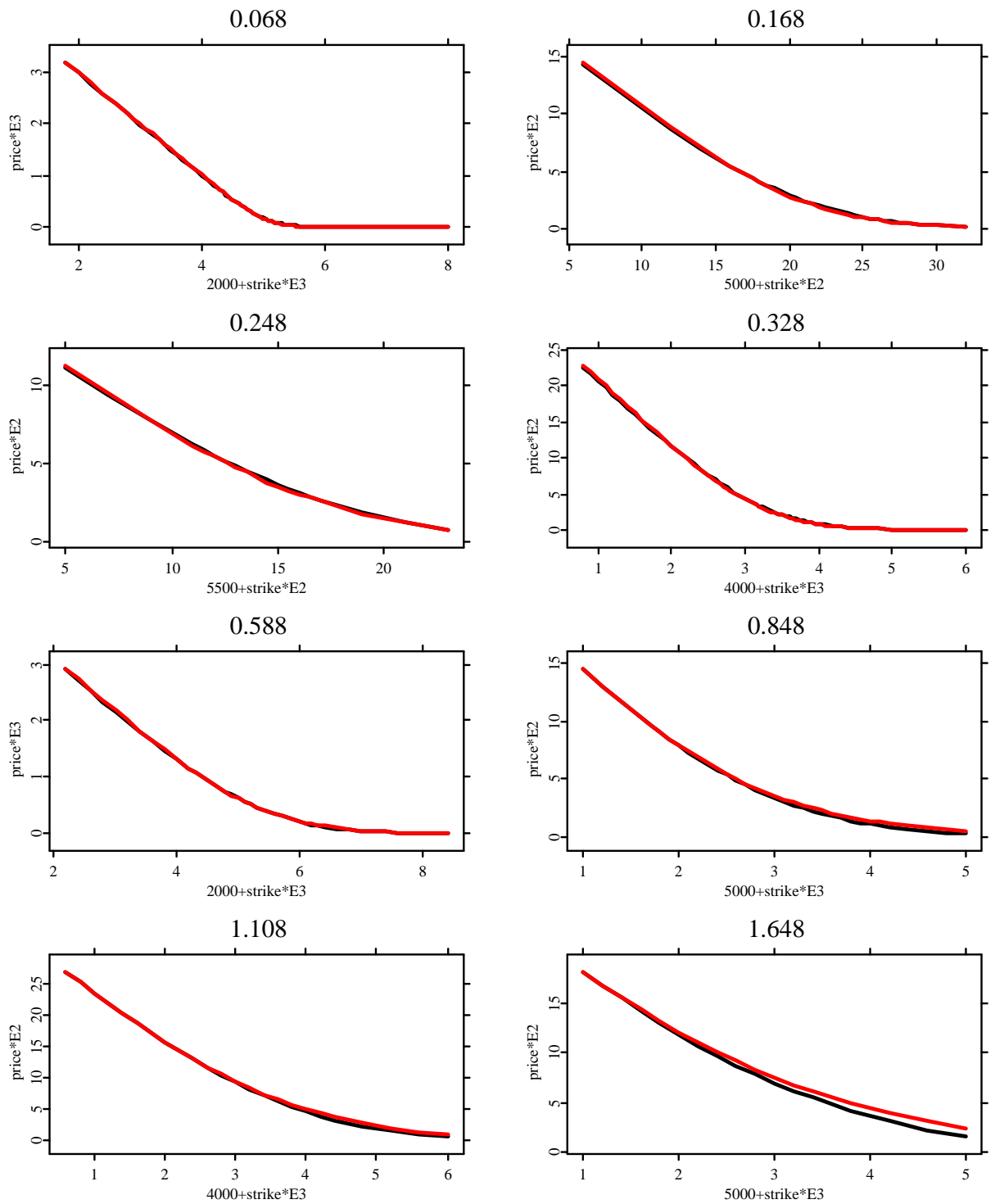


Figure 4.10: Observed and Merton model's price surface.

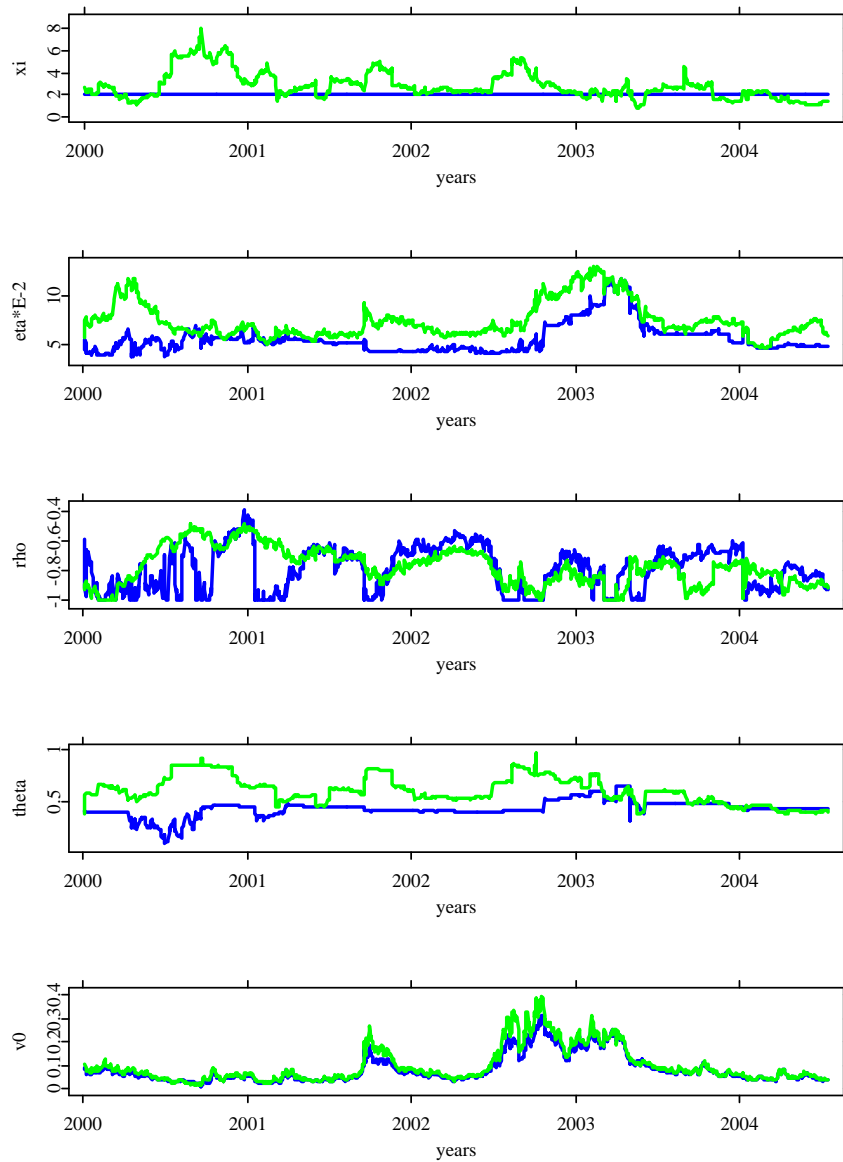


Figure 4.11: Parameter in Bates model (blue) and in the Heston model (green).

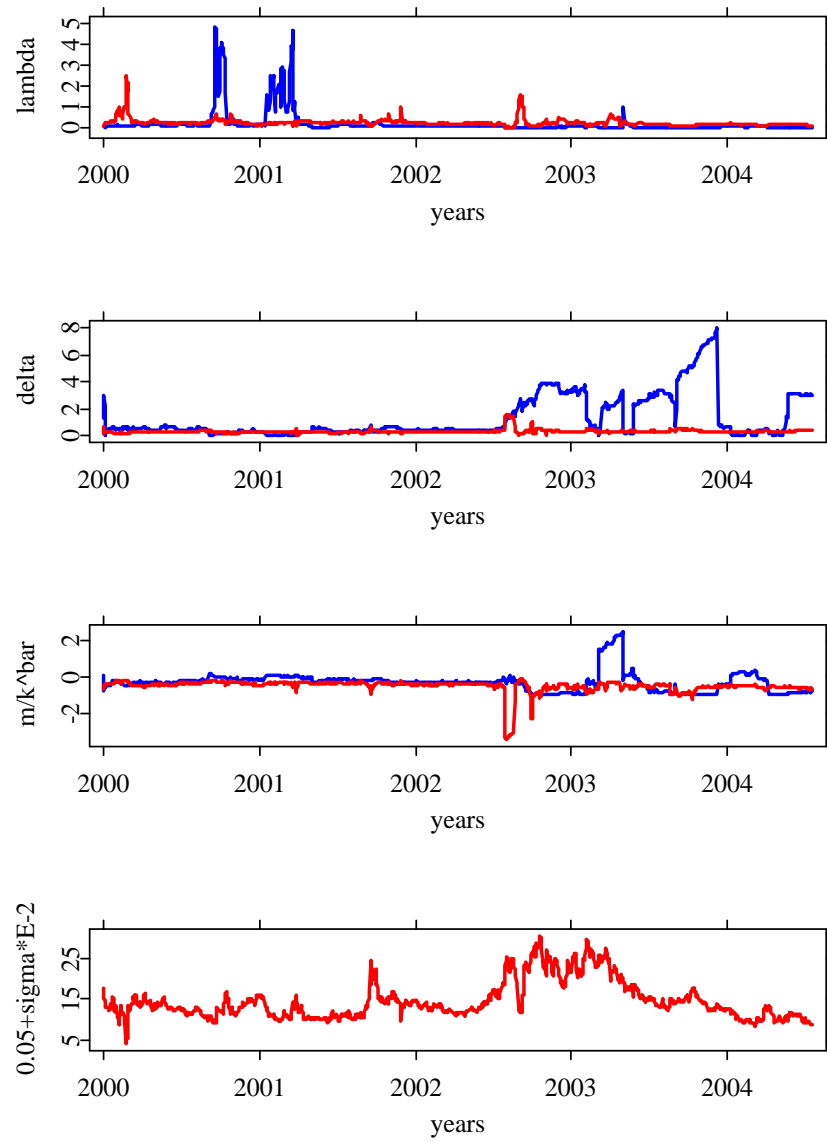


Figure 4.12: Parameter in Bates model (blue) and in the Merton model (red).

Chapter 5

Exotic options and Greeks

In this work, we analyze the dynamic hedging of exotic options. As there are many different kinds of exotic products we restrict ourselves to representative ones. To this end, we have chosen barrier options because these derivatives are among the simplest and most traded exotic options. In addition, we consider forward start barrier options in order to analyze also representatives of the class of forward start exotic options. These two types of derivatives will be described in Section 5.1.

As we consider the problem of hedging barrier options dynamically we have to decide on the dynamic hedging strategies. We choose from the variety of possibilities delta hedging and vega hedging. Thus we have to compute the greeks delta and vega. In order to evaluate these derivatives as difference quotient we apply Monte Carlo simulations which are described in Section 5.2. In this context, we analyze the correlation between barrier options and different products in order to use control variates for variance reduction.

In the last section, we describe approaches to calculate the Greeks by Monte Carlo methods. Moreover, we give representative results for the Greeks of options that expire normally or knock out before.

5.1 Barrier and forward start barrier options

Barrier options belong to the class of derivatives whose payoff depends on whether or not the underlying has crossed a specified level during the whole lifetime of the option. This specified level is called the barrier of the option. There are extensions to multiple barriers or multi crossings but we consider

in this work only simple barrier options.

For example, a down-and-out put option struck at K with maturity T and barrier B on the underlying (S_t) has the payoff

$$(K - S_T)^+,$$

if the value of the underlying was above B for all times $t < T$. The option is said to knock out when the value of the underlying falls below the barrier because the option does not pay anything in this case. Thus, the payoff is given by:

$$(K - S_T)^+ \mathbf{1}_{\{\min S_t > B\}}.$$

Similarly, a down-and-in call is determined by the payoff profile:

$$(K - S_T)^+ \mathbf{1}_{\{\min S_t < B\}}.$$

Such options are said to knock in. As the sum of these two options is a plain vanilla call (knock-out+knock-in=knockless) it is in general sufficient to consider only one type, say knock-out options. Moreover, there exist barrier options with payoff profiles of puts and all kinds of combinations.

As the payoffs are dominated by the corresponding plain vanilla payoffs barrier options are cheaper than plain vanilla options. This corresponds to the economic fact that they offer less rights. They are traded in the over-the-counter markets and are often demanded by speculators who have clear expectations about the future values of the underlying.

In the Black Scholes model, precise pricing formulas have been derived. For example, the value of a down-and-in put p_{di} with barrier B below strike K is given by:

$$\begin{aligned} p_{di} = & -S_0 \Phi(-x_1) + Ke^{-rT} \Phi(-x_1 + \sigma\sqrt{T}) + S_0 \left(\frac{B}{S_0}\right)^{2\lambda} \{\Phi(y) - \Phi(y_1)\} \\ & - Ke^{-rT} \left(\frac{B}{S_0}\right)^{2\lambda-2} \{\Phi(y - \sigma\sqrt{T}) - \Phi(y_1 - \sigma\sqrt{T})\} \end{aligned}$$

where

$$\begin{aligned}\lambda &= \frac{r + \sigma^2/2}{\sigma^2} \\ y &= \frac{\log\{B^2/(S_0K)\}}{\sigma\sqrt{T}} + \lambda\sigma\sqrt{T} \\ x_1 &= \frac{\log(S_0/B)}{\sigma\sqrt{T}} + \lambda\sigma\sqrt{T} \\ y_1 &= \frac{\log(B/S_0)}{\sigma\sqrt{T}} + \lambda\sigma\sqrt{T}\end{aligned}$$

See Hull (1997) for details.

Hence, the price of a down-and-out put is given by:

$$p_{do} = p - p_{di}$$

where p denotes the value of a plain vanilla call option.

So far we have discussed continuous barrier option. There are also discrete analogues where the barrier is monitored only at (finitely many) specified dates. In contrast to the continuous case there are in general no closed form pricing formulae. Therefore Broadie et al. (1997) have developed for the Black Scholes model the following approximation result:

$$p^d(B) = p(Be^{\pm\beta\sigma\sqrt{T/m}}) + o\left(\frac{1}{\sqrt{m}}\right) \text{ for } m \rightarrow \infty$$

where $+$ applies if $B > S_0$ and otherwise $-$, and $\beta \approx 0.5826$. Here $p^d(B)$ is the value of a discrete up-and-out put with barrier B and $p(B)$ is the price of a corresponding continuous barrier option.

In contrast, Joshi (2003) sees in the continuous barrier options already very good approximations to discrete (daily) barrier option. In the Bates model do not exist closed form pricing formulae for barrier options but we can price discrete barrier options by Monte Carlo simulation. If we had a result similar to Broadie et al. (1997) we could derive the prices for continuous barrier options. But there are hardly any truly continuous barrier options because the price of the underlying is only observable when trading takes place. Hence, we work with discrete barrier option as they are in general the relevant derivatives for traders.

Forward start options are options that are paid for at time t_0 but start at a later point of time $t_1 > t_0$. We will consider forward start barrier options

where at time t_0 the strike K and the barrier B are fixed relative to the price of the underlying at time t_1 . For example, we analyze forward start down-and-out puts that start in 1 year with a barrier $B = 0.8S_1$ and a strike $1.1S_1$ where S_1 denotes the value of the underlying in 1 year. We consider the case when they expiry in 2 years.

In this work, we analyze six types of barrier options: we consider down-and-out puts with relative barrier 0.8, relative strike 1.1 and time to maturity 1 (1y dop) and similar 2 years down-and-out puts with relative barrier 0.6 and relative strike 1.2 (2y dop). Moreover, we hedge up-and-out calls with relative barrier 1.2, relative strike 0.9 and time to maturity 1 (1y uoc) and also the analogue 2 years up-and-out calls with relative barrier 1.4 and relative strike 0.8 (2y uoc). In the class of forward start options we look at down-and-out puts with relative barrier 0.8 and relative strike 1.1 (fs dop) and up-and-out calls with relative barrier 1.2 and relative strike 0.9 (fs uoc). Both of these options start in 1 year and expire in 2 years.

5.2 Monte Carlo

In the Black Scholes model there are analytical formulae for the prices of barrier options. For the models that we consider in this work there are no such formulae or they still impose numerical problems. Hence, prices are often approximated in these models. We have chosen Monte Carlo methods to calculate the prices of the discrete barrier options described in the last section.

The price p of a discrete down-and-out put option is given by

$$E(X), \text{ where } X \stackrel{\text{def}}{=} \mathbf{1}_{\{\max S_{t_i} > B\}}(K - S_T)^+$$

and (S_t) is the price process of the underlying, K is the strike, B is the barrier, T is the maturity and t_i ($i = 1, \dots, n$) are the barrier times. A Monte Carlo estimator for this price is

$$\hat{p}_N \stackrel{\text{def}}{=} \frac{1}{N} \sum_{i=1}^N X_i$$

with independent random variables X_i that have the same distribution as X .

This estimator is unbiased and strongly consistent by the strong law of large numbers. Moreover, confidence intervals can be derived by the central

1y do p	2y do p	1y uo c	2y uo c	1y/2y fs do p	1y/2y fs uo c
0.8748	1.7889	0.8867	2.1431	0.9284	1.0592

Table 5.1: Standard errors for Bates prices (100000 simulations).

limit theorem. The standard error σ_X/\sqrt{N} implies an $\mathcal{O}(N^{-1/2})$ convergence rate which is independent of the dimension. The simple trapezoid rule for integration has in contrast a convergence rate of $\mathcal{O}(N^{-2/d})$ where d is the dimension. Thus, Monte Carlo methods become attractive only in high dimensions. As we have to sample paths (at discrete times) for (discrete) barrier options we face a high dimensional problem and hence use Monte Carlo simulation.

Broadie et al. (2004) have developed methods for sampling exact paths in the models that we consider. Nevertheless, we use discrete Euler approximations for the stochastic differential equations. These approximations introduce a bias that is controlled by the number of time steps. But the Euler scheme is simple to implement and computationally cheap.

The performance of the Monte Carlo simulations could be improved by more advanced approximations for the paths or by variance reduction techniques. We have used a technique based on control variates that is described in section 5.2.1.

We have calculated the prices of the six barrier options by 100000 simulations. The standard errors for the first simulation are given in table 5.1. They vary from option to option but are always below 1% because the option prices vary correspondingly.

In order to describe the option prices, figure 5.1 shows the prices of the six options per model. In all models the options with 2 years to maturity are the most expensive ones. In the Merton model the other four options have almost the same prices. In the Bates and the Heston model, the 1 years down-and-out puts have prices similar to the forward start down-and-out puts. Above these put prices lie the prices of the call options. Thus the prices are determined by the time to maturity most but also by the basic put/call feature is important. The calls are always in all models and for all types more expensive than the corresponding puts.

In figure 5.2 we compare the models for each option separately. We conclude that the prices for calls are similar in all models while the put

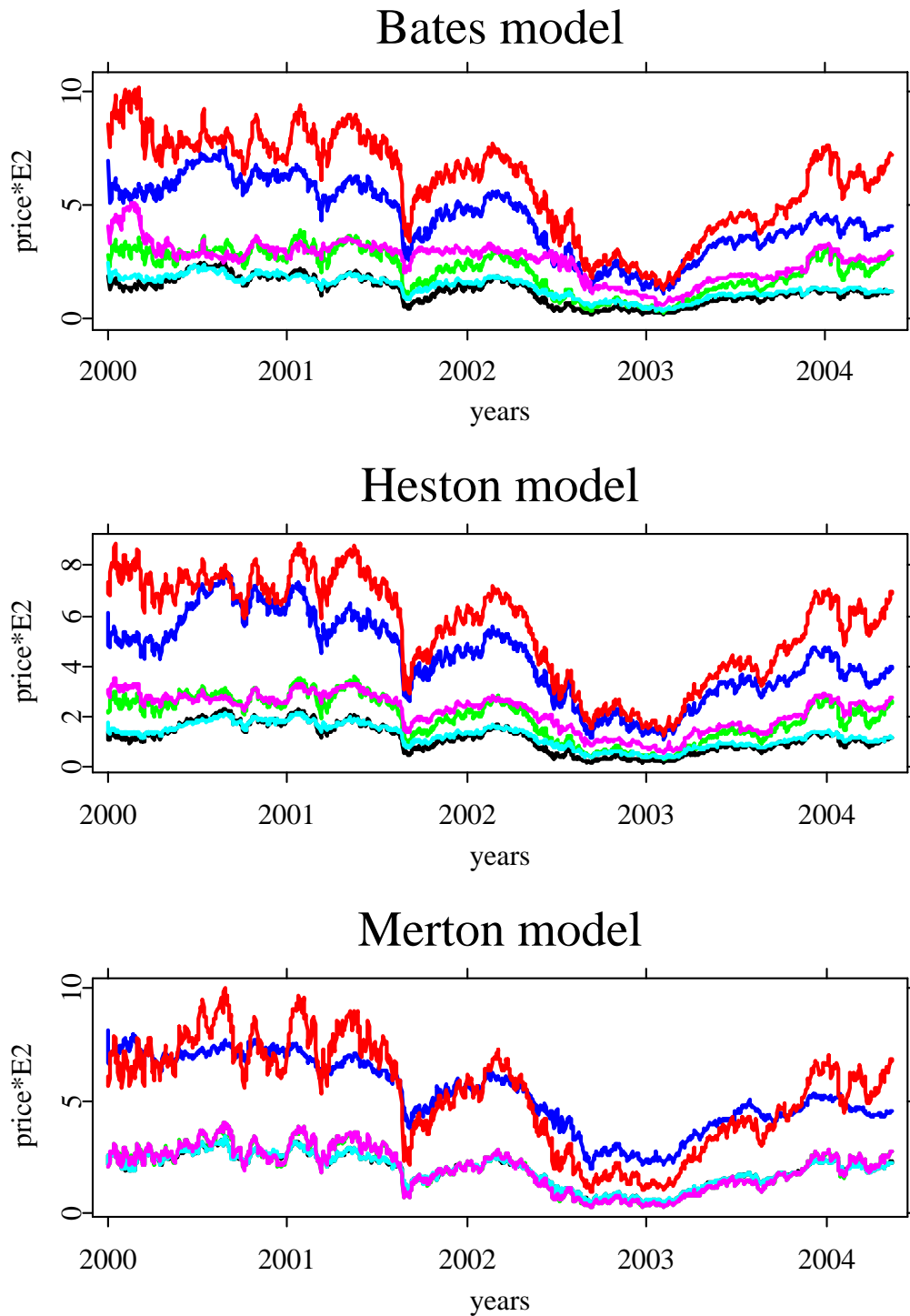


Figure 5.1: Prices of 1y dop (black), 2y dop (blue), 1y uoc (green), 2y uoc (red), fs dop (cyan) and fs uoc (magenta)

[batesbarrier.xpl](#) [hestonbarrier.xpl](#) [mertonbarrier.xpl](#)

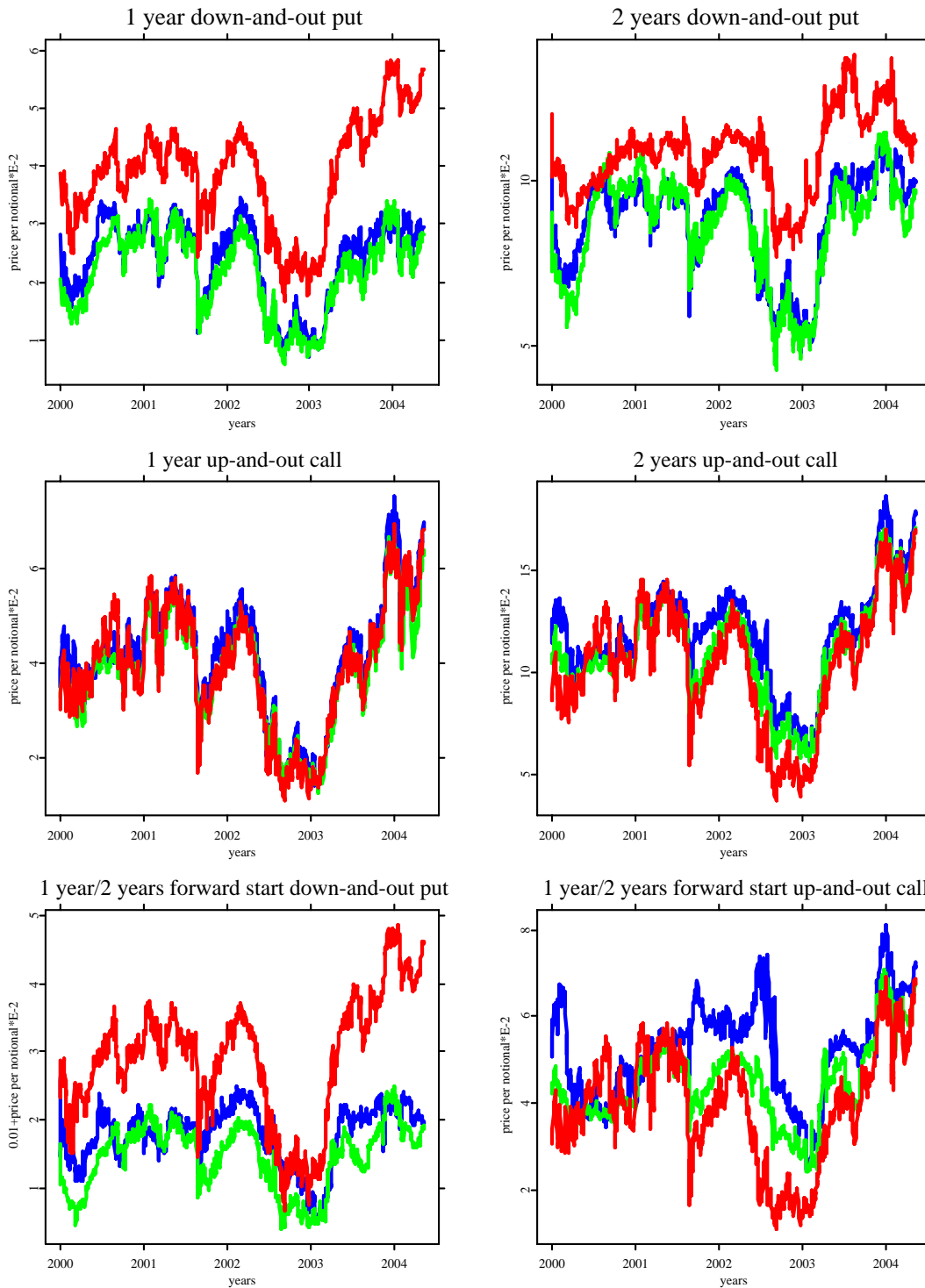


Figure 5.2: Option prices per DAX in the Bates model (blue), the Heston model (green) and in the Merton model (red)

	1y dop	2y dop	1y uoc	2y uoc	fs dop	fs uoc
Bates	0.8781	0.9261	0.8504	0.8910	0.9243	0.7992
Heston	0.8372	0.8951	0.8442	0.8729	0.8653	0.8381
Merton	0.8575	0.9534	0.8421	0.8577	0.8604	0.8434

Table 5.2: Correlation between option prices and DAX.

	1y dop	2y dop	1y uoc	2y uoc	fs dop	fs uoc
Bates	-0.9518	-0.9219	-0.9219	-0.8238	-0.7782	-0.3423
Heston	-0.9502	-0.9068	-0.9285	-0.8676	-0.8745	-0.6937
Merton	-0.8756	-0.6085	-0.9376	-0.9418	-0.8788	-0.9385

Table 5.3: Correlation between option prices per notational and at the money implied volatilities with mean time to maturity.

prices in the Merton are higher than in the others models. Thus, we see again that the type of option is important.

In order to compare the option prices with the underlying we have calculated the corresponding correlations in table 5.2. Although the correlation are high we have an even higher linear dependence between the option prices per notional and at the money implied volatilities with mean time to maturity. These results are given in table 5.3.

5.2.1 Control variates

Control variate methods use information about estimation errors of known quantities to reduce the variance of estimators of unknown quantities.

Suppose the expectation $E(Y)$ of a random variable Y is to be calculated. The simple Monte Carlo estimator is $\bar{Y} = (Y_1 + \dots + Y_n)/n$ for n independent replications Y_i of Y . If we have in addition n independent observations X_1, \dots, X_n of a random variable X with known mean $E(X)$ then we can

calculate for any fixed c :

$$Y_i(c) = Y_i - c\{X_i - E(X)\}$$

and estimate $E(Y)$ by the mean:

$$\bar{Y}(c) = \bar{Y} - c\{\bar{X} - E(X)\} = \frac{1}{n} \sum_{i=1}^n [Y_i - c\{X_i - E(X)\}]$$

This mean is called a control variate estimator for $E(Y)$ because the errors $X_i - E(X)$ serve as controls. Multiple control variates estimators can be treated in a similar way but we illustrate the idea only for one control.

Control variate estimators are unbiased and strongly consistent. The coefficient c is chosen such that the variance of $\bar{Y}(c)$ is minimal. As the variance is given by:

$$\begin{aligned} \text{Var}\{\bar{Y}(c)\} &= \text{Var}\left[\frac{1}{n} \sum_{i=1}^n [Y_i - c\{X_i - E(X)\}]\right] \\ &= \frac{1}{n} \text{Var}[Y - c\{X - E(X)\}] \\ &= \frac{1}{n} (\sigma_Y^2 - 2c\sigma_X\sigma_Y\rho_{XY} + c^2\sigma_X^2) \end{aligned}$$

the optimal coefficient c^* that minimizes the variance of the control variate estimator is given by:

$$c^* = \frac{\sigma_Y}{\sigma_X} \rho_{XY} = \frac{\text{Cov}(X, Y)}{\text{Var}(X)}$$

This parameter gives also the slope of the linear regression. Using this optimal value results in the variance reduction

$$\text{Var}\{\bar{Y}(c^*)\} = (1 - \rho_{XY}^2) \text{Var}(\bar{Y})$$

and thus the reduction works the better the stronger the correlation is. If the quantities $\text{Cov}(X, Y)$ and $\text{Var}(X)$ are unknown c^* has to be estimated and this introduces some bias.

In the last section, we have calculated the prices of different options. As the prices are given as expectations we have used Monte Carlo methods. For variance reduction we have employed control variates. The only necessary condition for a control is that its expectation is known. Thus we have considered barrier options in the Black Scholes model, the price of the underlying

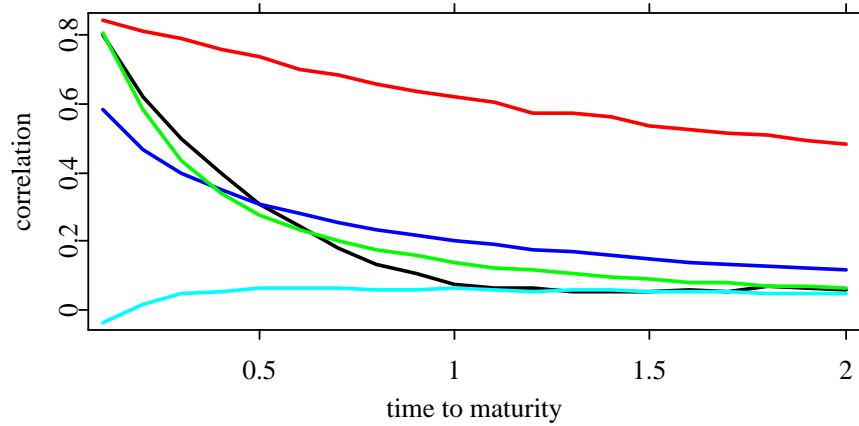


Figure 5.3: Correlation of the 1 year down-and-out put barrier option and the control variates: Black Scholes barrier (black), underlying (blue), European put (green), butterfly spread (red) and option with final barrier payoff (cyan).

and European puts as controls. Moreover, we analyzed combinations of European puts that resemble the final payoff of our barrier options, e.g. the final payoff of 1 year down-and-out put is $\mathbf{1}_{\{S_1 > B\}}(K - S_1)^+$. Finally, we have considered a butterfly spread between the barrier B and the strike K . The exact prices of these products are known and thus they can be used as control variates.

Their effectiveness in variance reduction is measured by the correlation which is illustrated in figure 5.3 for the 1 year down-and-out barrier option. The highest correlation has butterfly spread, the other possible controls hardly reduce the variance. Moreover, multiple controls do not improve the result of the butterfly spread. The figure illustrates further how the correlation and thus the variance reduction decreases with increasing time to maturity.

As we calculate derivatives of option prices by difference quotients in the next section we state here the variance reduction for the differences. It is shown in figure 5.4. While the high correlation of the butterfly corresponds to the results above the variance reduction of the option with final barrier payoff was not motivated by the last figure. Thus it is neither sufficient nor necessary for good control variate of the difference to have a high correlation to the price.

We illustrate the final variance reduction in figure 5.5 by plotting $1 - \rho_{XY}$.

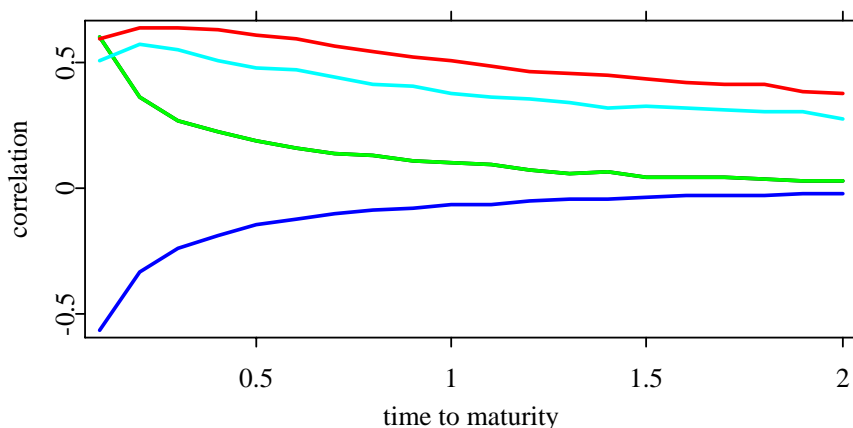


Figure 5.4: Correlation of the differences of the control variates and the differences of the 1 year down-and-out barrier option; Black Scholes barrier (black), underlying (blue), European put (green), butterfly spread (red) and option with final barrier payoff (cyan).

The graph shows that the reduction is smaller for the differences than for the prices directly.

5.3 Greeks

Traders try to reduce the risk of portfolios by making them immune to changes in variables like the underlying. To this end, they often hedge dynamically on the basis of the Greeks. These factor sensitivities measure how the portfolio's market value responds to a change in some variable, e.g. the underlying. There are five Greeks but we will consider only the following two:

- δ measures first order (linear) sensitivity to an underlying
- \mathcal{V} measures first order (linear) sensitivity to the volatility of an underlying

There are different methods to estimate the Greeks. Suppose we consider an option with price $\alpha(\theta) = \mathbb{E}\{f(\theta)\}$ where f is the discounted payoff. We want to calculate the derivative $\alpha'(\theta)$ with respect to θ .

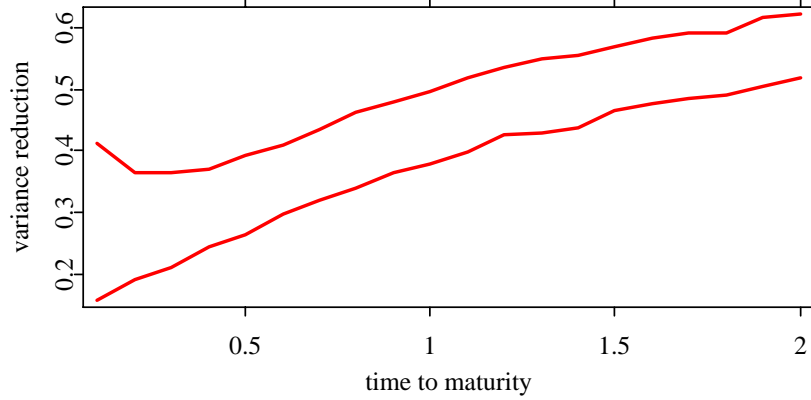


Figure 5.5: variance reduction using butterfly spreads as control variates for differences (upper line) and prices (lower line)

The pathwise method assume that differentiation and integration can be interchanged and estimates the derivative by:

$$\alpha'(\theta) = E\left\{\frac{d}{d\theta}f(\theta)\right\}$$

The knock-out feature of the discrete barrier options that we consider makes the payoff discontinuous in the path of the underlying and basically this makes the pathwise method not applicable in our situation.

In the likelihood method, the payoff f is modelled by a payoff profile F and a random variable X . Moreover, it is assumed that X has a density g_θ that depends on a parameter θ . An interchange of differentiation and integration leads to:

$$\alpha'(\theta) = \int F(x) \frac{d}{d\theta} g_\theta(x) dx = E\left\{F(X) \frac{g'_\theta(X)}{g_\theta(X)}\right\}$$

Broadie et al. (2004) have applied these methods in our models for calculating the Greeks. Their idea was to condition the expected payoff on the volatility path in order to extend the Black-Scholes setting of lognormal random variables. This approach leads to unbiased Monte Carlo estimators but it is computationally expensive and not straightforward to implement.

Another method that also leads to unbiased Monte Carlo estimators can be derived by Malliavin calculus. This approach has been described e.g. by

Davis & Johansson (2004). But it is again computationally quite expensive.

Instead of these advanced techniques we have used the simple approximation by a difference quotient. Thus, we approximate δ by:

$$E\left[\frac{(K - S_T^{+h})^+ \mathbf{1}_{\{\min S_t^{+h} > B\}} - (K - S_T^{-h})^+ \mathbf{1}_{\{\min S_t^{-h} > B\}}}{2h}\right]$$

where $(S_t^{\pm h})$ is the process of the underlying with $S_0^{\pm h} = S_0 \pm h$. Similarly, we approximate \mathcal{V} by changing the start parameter of the volatility process. There are different possibilities to calculate these Greeks, e.g. \mathcal{V} could be estimated by moving the average level instead of the starting value of the volatility.

A drawback of this approach can be seen in the bias and the dependence on the parameter h . Moreover, h cannot be chosen in absolute terms but has to consider the distance of barrier from the underlying. Therefore, the choice of h is also problematic.

Our approach of estimating a Greek requires one Monte Carlo. Writing the estimator as:

$$\frac{E[(K - S_T^{+h})^+ \mathbf{1}_{\{\min S_t^{+h} > B\}}] - E[(K - S_T^{-h})^+ \mathbf{1}_{\{\min S_t^{-h} > B\}}]}{2h}$$

we see that our approximation could also be calculated by two simulations, one for each expectation. But this approach leads to two simulation errors which are afterwards subtracted. This combination of errors gives unacceptable results in general. Hence, one performs only one Monte Carlo simulation. Thus control variates for Greeks have to be correlated to the difference of the prices. A correlation with the price alone is not important.

Monte Carlo simulations do not permit to calculate the daily Greeks for all options because the simulations take too long. Thus we have restricted ourselves to start every week all six options and to calculate the Greeks once a week. Nevertheless we check every day if the option has been knocked out or not. This is illustrated in figures 5.6 and 5.7. The option considered for the first graphic knocks out. The Greeks rise sharply before this event. In the second figure the options expires and the Greeks show no abrupt movements until 3 months before expiry \mathcal{V} starts to change rapidly.

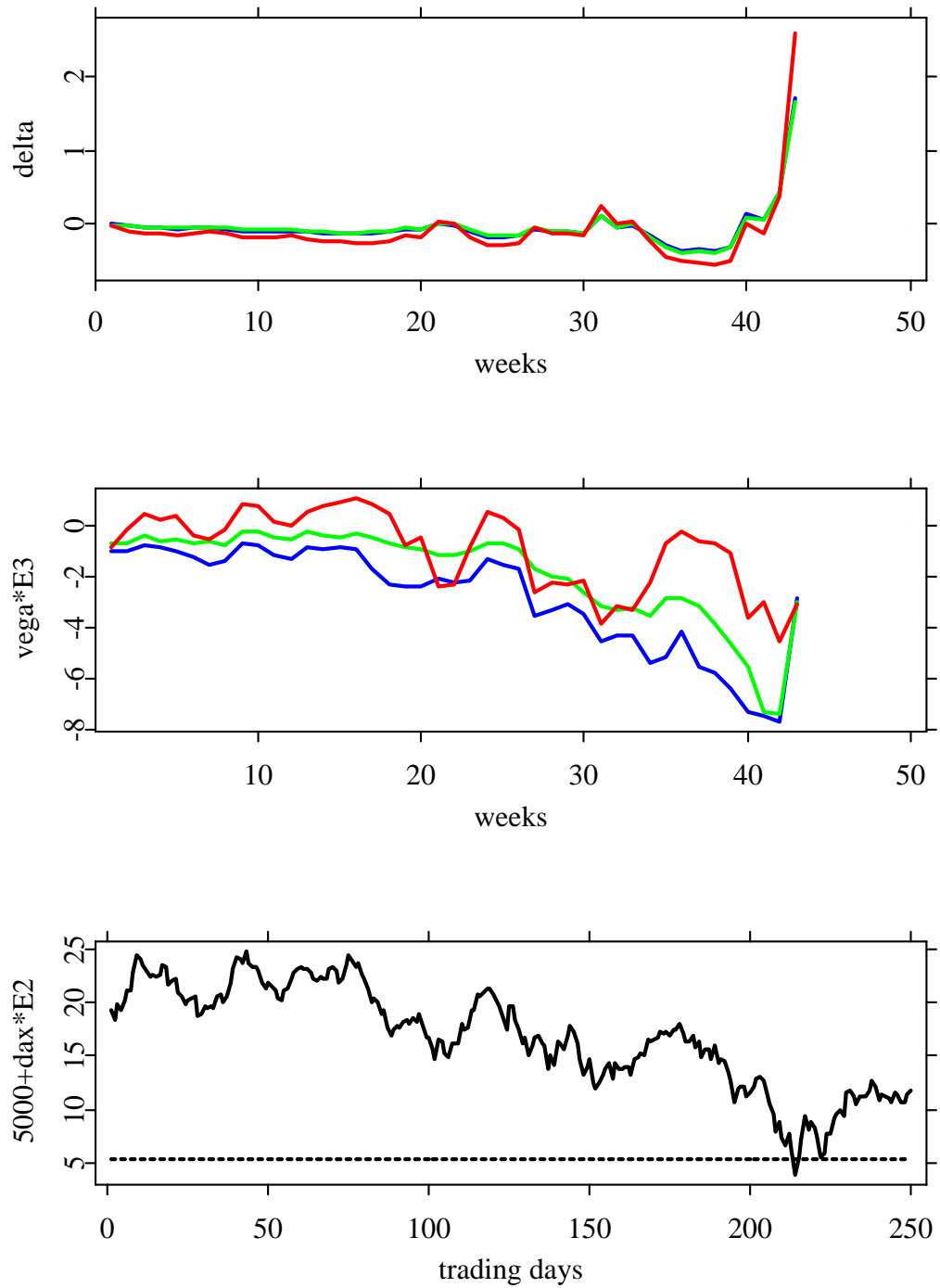


Figure 5.6: Greeks for a down-and-out put that knocks out.

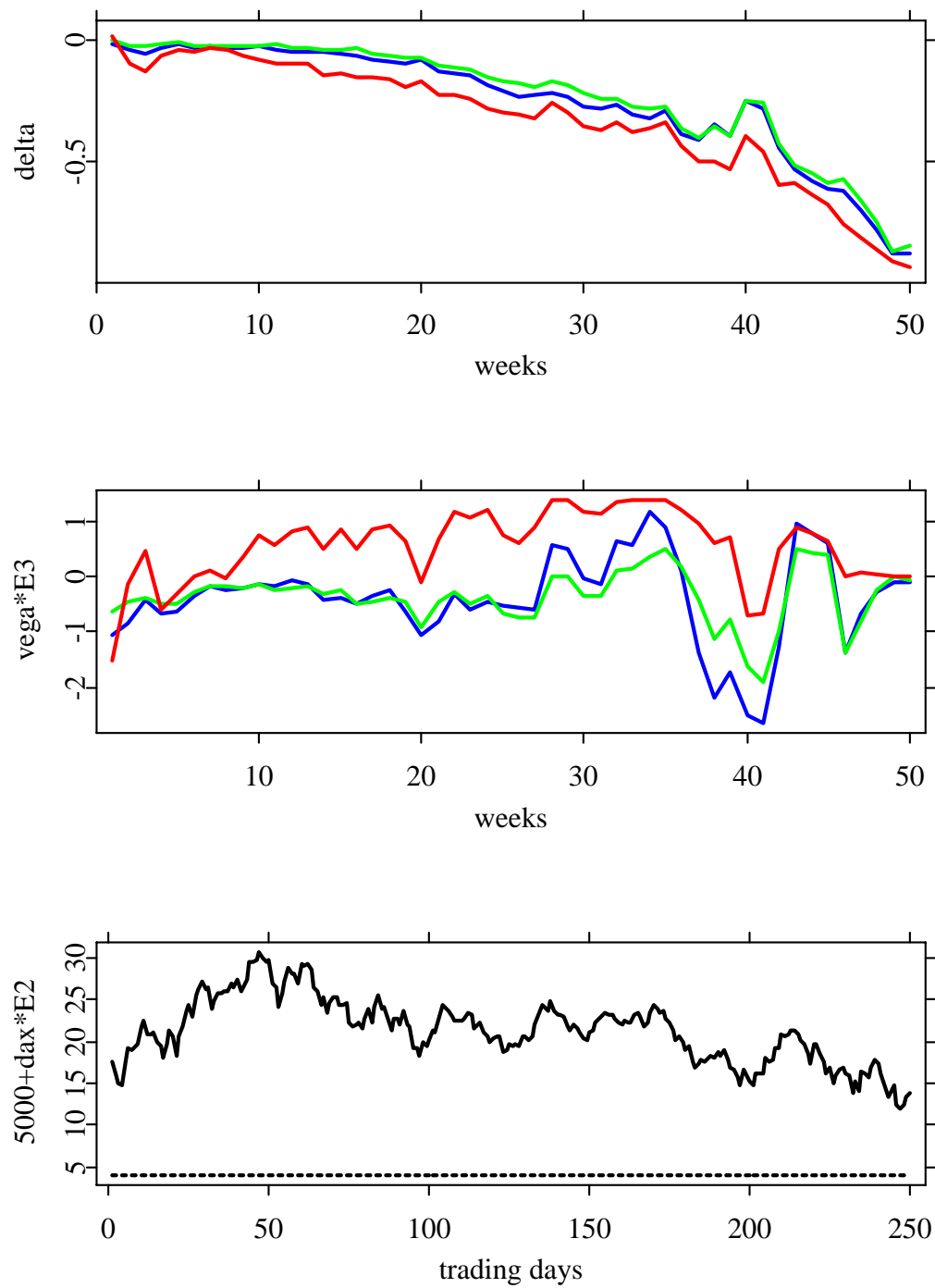


Figure 5.7: Greeks for a down-and-out put that expires normally.

Chapter 6

Dynamic hedging

In this chapter, we consider the hedging performance of the three models. We analyze three dynamic hedging schemes on the basis of the Greeks: delta hedging, vega hedging and for the two factor models delta hedging with minimum variance.

The delta hedging aims to reduce the risk of price movements of the underlying. To this end, the underlying is bought and sold according to the Greek δ which is the derivative of the option price with respect to the price of the underlying. We consider at the beginning a short position in the barrier option. Thus we buy δ shares of the underlying. When we hedge again a week later we adjust the number of shares to the new δ of the barrier option. When the barrier is hit or when the option expires we clear our position. This strategy leads to the cumulative hedging cost which have summed up over the hedging period.

In a vega hedge one takes a position in the underlying and in another option O . In this way one tries remove also the volatility uncertainty which is another source of risk in stochastic volatility models. To this end, we buy $\mathcal{V}_O^{-1}\mathcal{V}_B$ options O where $\mathcal{V}_O(\mathcal{V}_B)$ is the vega of the option O (the barrier option). This makes our portfolio vega-neutral. In order to remove also the delta risk we perform a normal delta hedge for our portfolio. We apply vega hedging only until two months before expiry because the vega becomes numerically unstable at the end. In the last two months we therefore use only delta hedging.

The delta hedging with minimum variance tries to remove the risk of movements in the underlying but at the same time it aims to minimize the profit and loss variance. It is defined for stochastic volatility models and uses a modified delta instead of the usual one, see Matytsin (2000) for details.

We have used these three hedging methods in the three models for our six options. The results are shown in the following figures where we have measured the hedging cost per notional. Here the notional is the price of the underlying. Thus negative cumulative hedging errors represent profits of the hedge.

In order to measure the hedging in the model we have subtracted at the beginning the price of the barrier that we are short. This allows us to check if the hedging gives the model price in the mean. Moreover, we can analyze the general hedging performance by considering the variance of the hedging errors.

For all options the results of the different hedging methods lead to similar results which may indicate that the vega should be calculated differently to obtain a bigger impact. The hedging of the 1 year down-and-out put option leads in all models almost to a point distribution with two outliers. The outliers represent two expensive hedges. But the median and the mean of the distribution are negative. Thus the model prices seem to be too big and the hedging works well. For the corresponding options with 2 years to maturity the distributions are similar but without outliers. Hence the hedging performance is even better. The 1 and 2 year up-and-out call options lead both to bimodal distributions with outliers. In these cases the mean and median are more negative than for the puts. Thus the model prices may be too high in terms of dynamic hedging. The forward start options permit also good dynamic hedging but the mean and median are again negative.

Based on the hedging performance for exotic options all the models perform well but the stochastic volatility models tend have error distributions with only one mode.

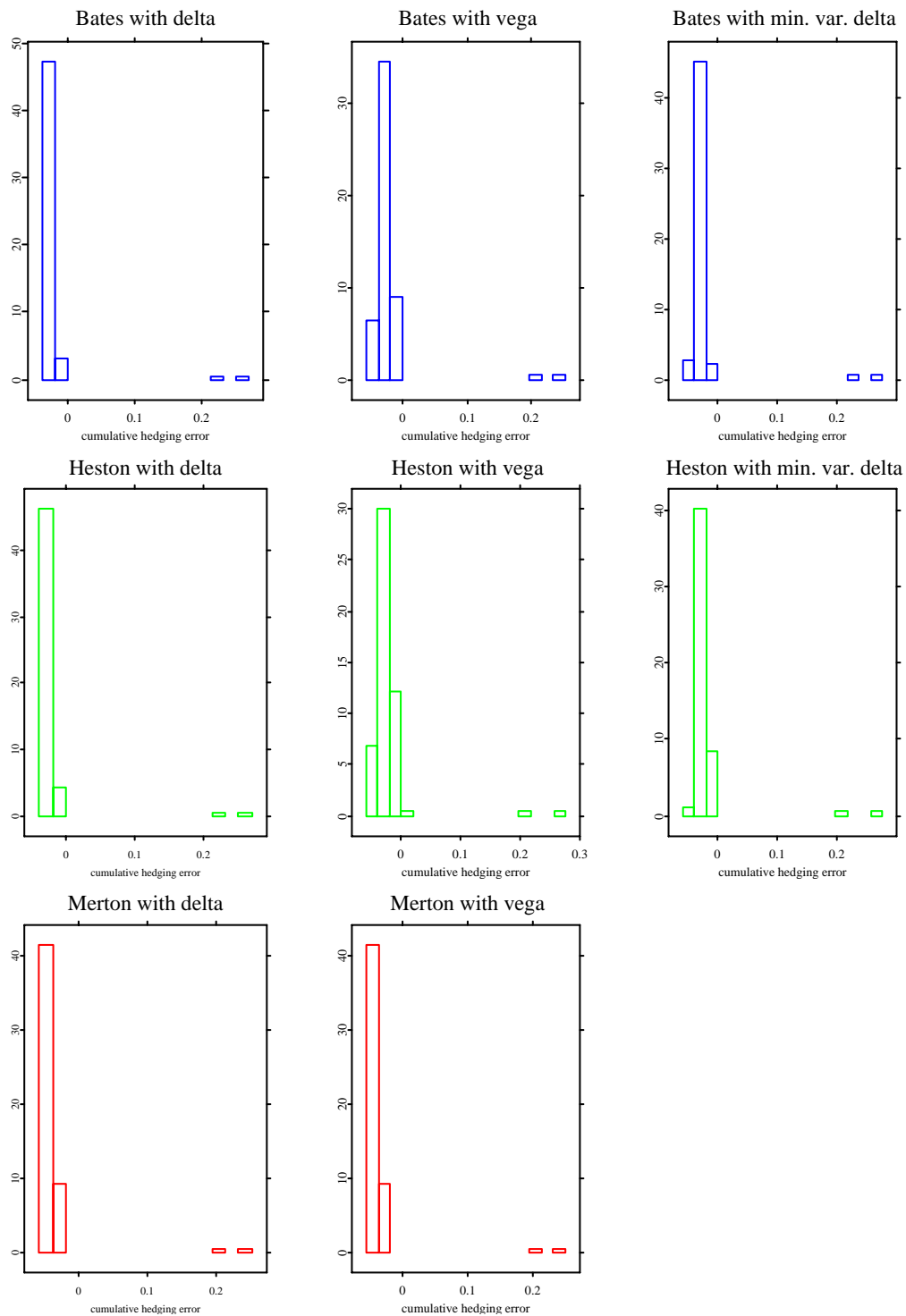


Figure 6.1: Hedging results for 1y dop.

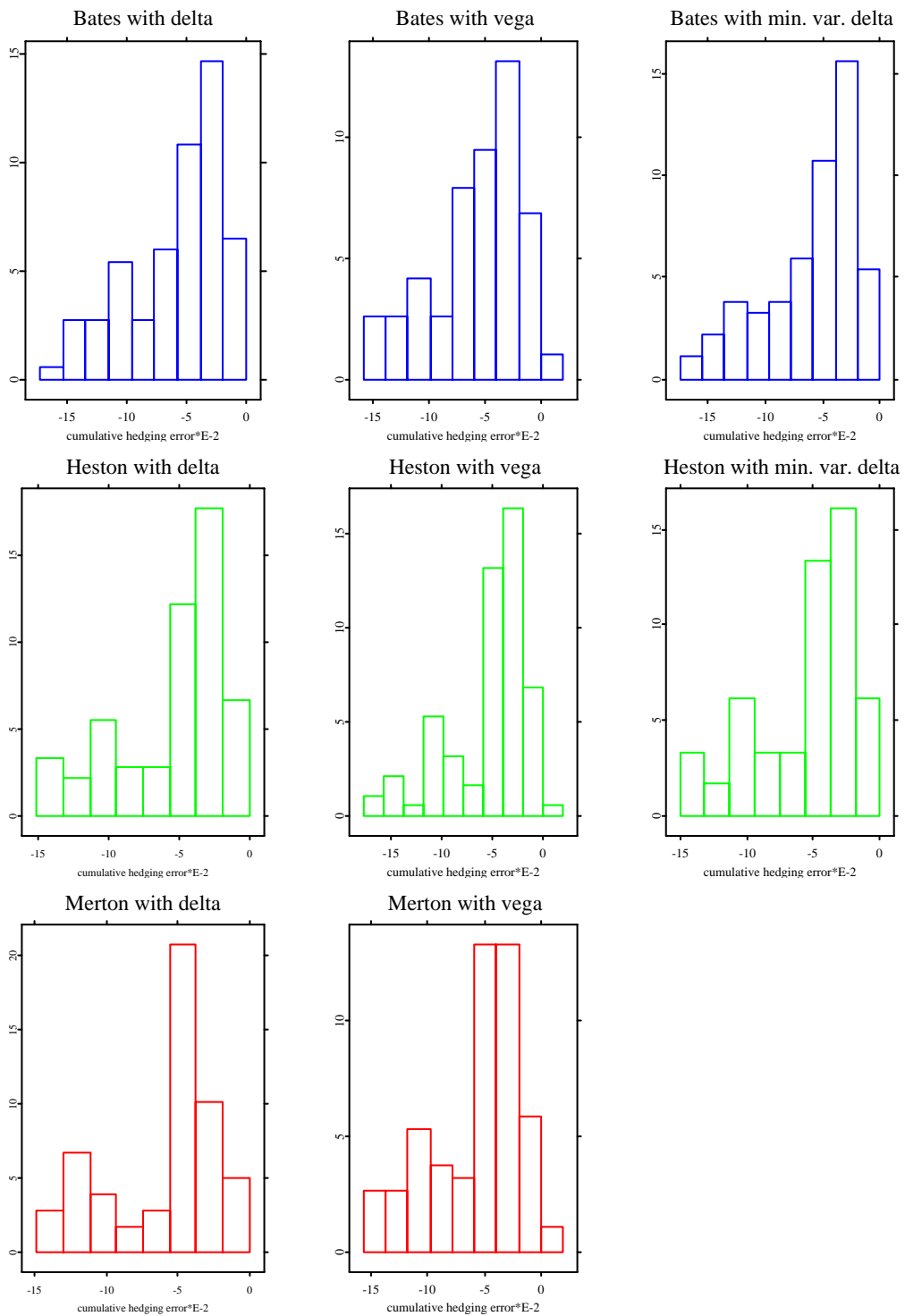


Figure 6.2: Hedging results for 2y dop.

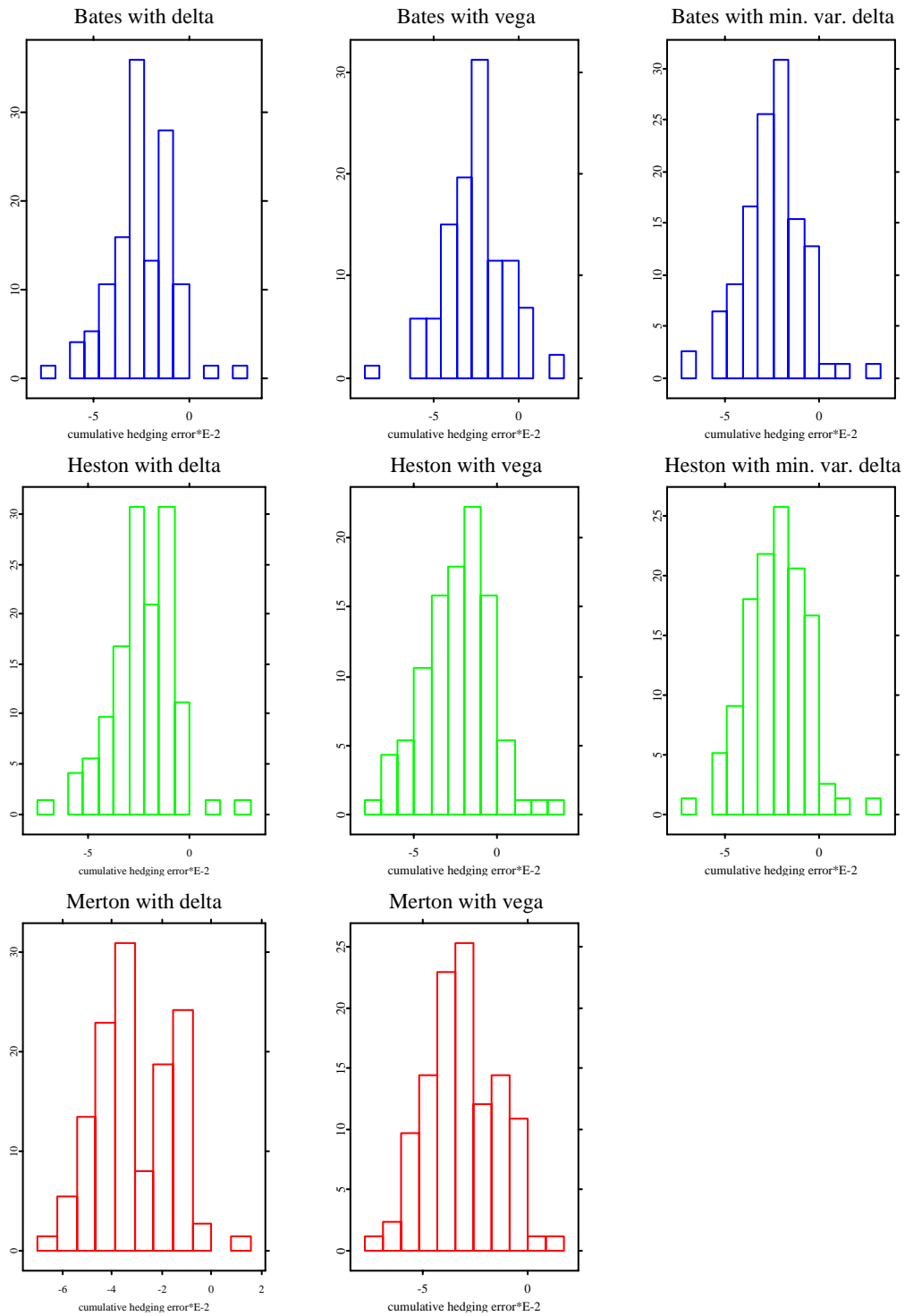


Figure 6.3: Hedging results for 1y uoc.

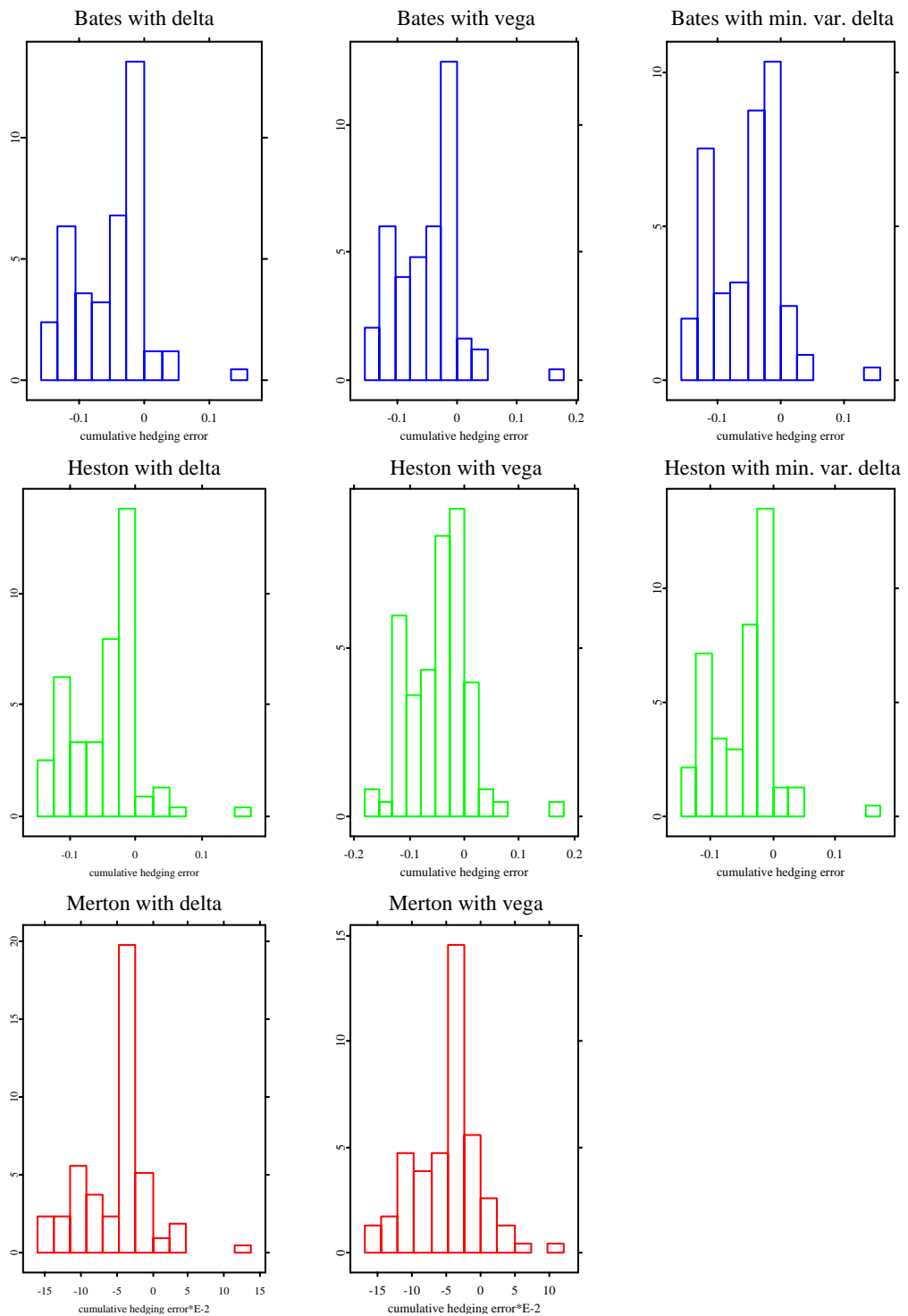


Figure 6.4: Hedging results for 2y uoc.

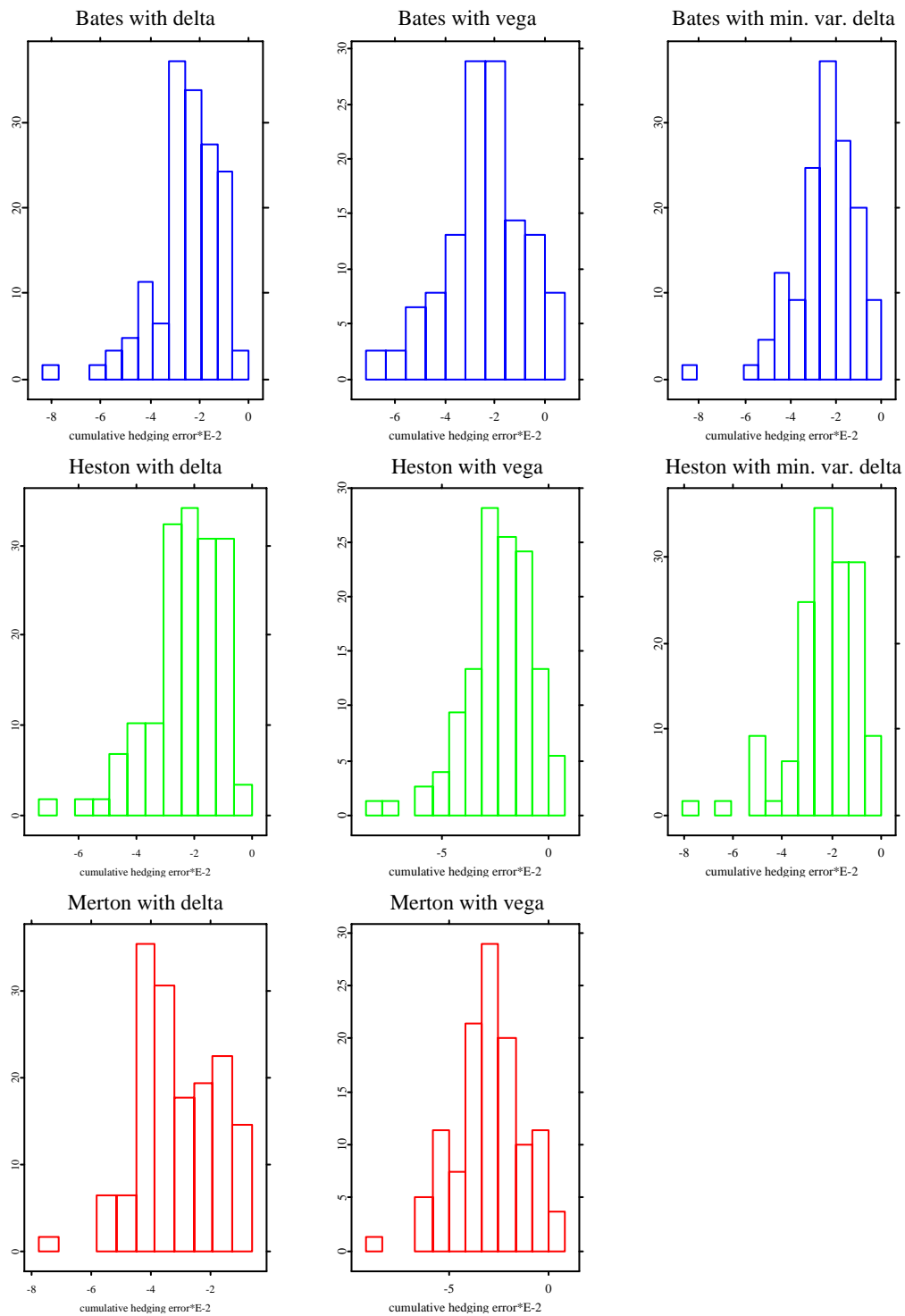


Figure 6.5: Hedging results for fs dop.

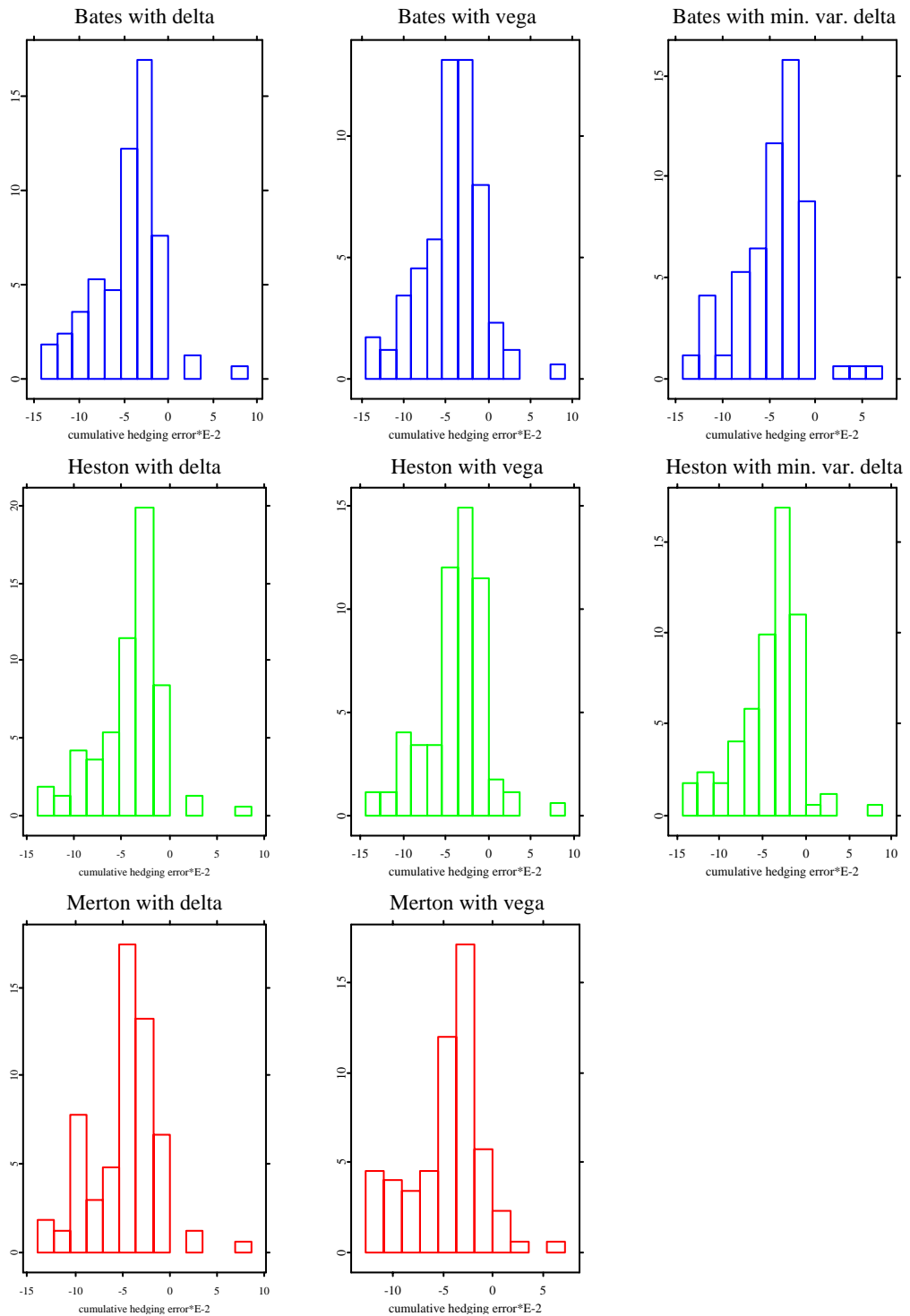


Figure 6.6: Hedging results for fs uoc.

Chapter 7

Conclusion

In this work, we have compared the Merton, the Heston and the Bates model.

To this end, we have first calibrated the models to the data. The Bates model provided the best fit to the data. This can be explained by the fact that it is a generalization of the other two models. While the Heston model's fit was almost as good as the Bates model's, the Merton model gave a considerably worse fit. Thus the stochastic volatility model performs better than the jump diffusion model for replicating the observed surfaces.

Considering the stability of parameters we found out that the Bates has too many parameters to guarantee their stability. Reducing the number of parameters in the Bates model by setting a parameter to a constant, we have improved the stability but not overcome this problem. The Heston model on the other hand had stable parameters that do not seem to be influenced by numerical problems. The Merton model has the smallest number of parameters. They were more stable than the parameters in the Bates model but seemed to be influenced by numerical problems.

We have found these results by the simulated annealing algorithm. This method turned out to be faster and more accurate than a gradient based method. Moreover, this optimization routine has the merit of not getting trapped in a local minimum so that it can find a global solution. But our analysis could be extended to different periods and other optimization methods like differential evolution.

After the calibration, we have calculated the prices and the Greeks of six barrier options. It turned out that the option prices increase with the time to maturity if the others characteristics like barriers, etc are adjusted accord-

ingly. Moreover, calls seem to be more expensive than puts in all models. In addition, we found out in our Monte Carlo simulation that butterfly spreads are sufficiently correlated with barrier options to be used as control variates for the prices or the differences of the prices.

In our dynamic hedging study, we saw that this technique works rather well even for simple delta hedging. This result is not supported by theory which prefers static hedges for discrete barrier options. The other hedging approaches did not lead in general to better results. This suggests that the vega should be calculated differently to get a significant impact for delta hedging with minimum variance and for vega hedging.

As we have calculated the Greeks by Monte Carlo methods we had to restrict ourselves to a low hedging frequency. The importance of the hedging frequency could be analyzed in another study with a different implementation of pricing, e.g. by finite difference methods.

Comparing our work to literature we can conclude that the results of Bakshi et al. (1997) also hold for exotic options: The Heston model gives a good fit to the data, it has stable parameters and gives reasonable hedging results. We have not found exactly the same results as Schoutens et al. (2004). Some of the options considered in this study had similar prices in all models. But the prices of other options differ across the models. This holds especially for the down-and-out put options. Because of the stock market crash on 11/09/2001 many of these options knocked out and this extreme event may thus have influenced our results.

We conclude that stochastic volatility models have a good overall performance and the use of jump diffusion models is not supported by our study. It suggests rather that stochastic volatility models with jumps in the spot and jumps in the volatility are overparametrized because the parameters of the Bates model are already unstable.

XploRe quantlets

The following quantlets have been produced for this work:

-  `batessim.xpl`
-  `hestonsim.xpl`
-  `mertonsim.xpl`
-  `volasim.xpl`
-  `batesbarrier.xpl`
-  `hestonbarrier.xpl`
-  `mertonbarrier.xpl`

Bibliography

- Bachelier, L. (1900). Théorie de la spéculation, *Annales de l'Ecole Normale Supérieure III* 17: 21–86.
- Bakshi, G., Cao, C. & Chen, Z. (1997). Empirical Performance of Alternative Option Pricing Models, *The Journal of Finance* 5: 2003-2049.
- Bates, D., (1996). Jump and Stochastic Volatility: Exchange Rate Processes Implicit in Deutsche Mark Options, *Review of Financial Studies* 9: 69-107.
- Black, F. & Scholes, M. (1999). The pricing of options and corporate liabilities, *Journal of Political Economy* 81: 637–659.
- Borak, S., Detlefsen, K., & Härdle, W. (2004). FFT based option pricing, *Statistical Tools for Finance and Insurance*, Springer, Berlin.
- Broadie, M., Glassermann, P. & Kou, S.G. (1997). A continuity correction for discrete barrier options, *Mathematical Finance* 7: 325-349
- Broadie, M. & Kaya, Ö. (2004). Exact Simulation of Stochastic Volatility and other Affine Jump Diffusion Processes. Working paper, Columbia University, New York.
- Broadie, M. & Kaya, Ö. (2004). Exact Simulation of Option Greeks under Stochastic Volatility and Jump Diffusion Models, *Proceedings of the 2004 Winter Simulation Conference*.
- Carr, P. & Madan, D. (1999). Option valuation using the fast Fourier transform, *Journal of Computational Finance* 2: 61–73.
- Cont, R., (2001). Empirical properties of assets returns: Stylized facts and statistical issues, *Quantitative Finance* 1: 1-14.

- Cont, R. & Tankov, P. (2004). *Financial Modelling With Jump Processes*, Chapman & Hall/CRC.
- Davis, M. & Johansson, M. (2004). Malliavin Monte Carlo Greeks for jump diffusions. Working paper, Imperial College, London.
- Derman, E. & Kani, I. (1994). Riding on a smile, *Risk* 7 (2) : 32-39.
- Fengler, M., (2004). Arbitrage-free smoothing of the implied volatility surface. Working paper.
- Franke, J., Härdle, W. & Hafner, C. (2004). *Introduction to Statistics of Financial Markets*, Springer, Berlin.
- Glassermann, P. (2004). *Monte Carlo Methods in Financial Engineering*, Springer, New York.
- Green, P.J. & Silverman, B.W. (1994). *Nonparametric regression and generalized linear models*, Vol. 58 of Monographs on Statistics and Applied Probability, Chapman and Hall, London.
- Hafner, R. & Wallmeier, M. (2001). The dynamics of DAX implied volatilities, *International Quarterly Journal of Finance* 1: 1-27.
- Heston, S., (1993). A closed-form solution for options with stochastic volatility with applications to bond and currency options, *Review of Financial Studies* 6: 327-343.
- Hull, J., (1997). *Options, futures, and other derivatives*, third international edition, Prentice Hall, London.
- Joshi, M. S., (2003). *The Concepts and Practice of Mathematical Finance*, University Press, Cambridge.
- Kahale, N., (2004). An arbitrage-free interpolation of volatilities, *Risk magazine*.
- Lee, R., (2004). Option pricing by transform methods: extensions, unification and error control, *Journal of Computational Finance* 7: 51-86.
- Madan, D., & Milne, F. (1991). Option pricing with variance gamma martingale components, *Mathematical Finance* 1: 39-55.
- Matytsin, A., (2000). Stochastic Volatility and Jump Diffusion In Equity Markets, *Merril Lynch*.

Merton, R., (1976). Option pricing when underlying stock return are discontinuous, *Journal of Financial Economics* 3: 125-144.

Samuelson, P., (1965). Rational theory of warrant pricing, *Industrial Management Review* 6: 13-31.

Schoutens, W. , Simons, E. & Tistaert, J. (2004). A Perfect Calibration! *Wilmott magazine*.